TAMPEREEN TEKNILLINEN YLIOPISTO
TAMPERE UNIVERSITY OF TECHNOLOGY

MD TANJIMUDDIN

REACTIVE POWER CONTROL IN GRID-CONNECTED CONVERTER

Master of Science thesis

Examiner: Asst. Prof. Tuomas Messo
Examiner and topic approved by the
Faculty Council of the Faculty of
Computing and ELectrical Engineering
on 1st October 2018

ABSTRACT

MD TANJIMUDDIN: Reactive power control in grid-connected converter
Tampere University of Technology
Master of Science thesis, 64 pages, 1 Appendix page
September 19, 2018
Master's Degree Programme in Electrical Engineering
Major: Smart Grid
Examiner: Asst. Prof. Tuomas Messo
Keywords: Reactive power, Droop control, Grid-connected converter, Point of common coupling

During the last two decades, power system engineers are much concerned about the quality of power that is being supplied to the customers. Power losses at the lower level, compensating devices to balance the active and reactive power and overall stability of the power system is demanded. Thus, the present power system is now undergoing a severe transformation and expansion due to the available smart technologies, the evolution of renewables and for the rapid increase of electricity demands. Power electronics technology plays a vital role in the integration of renewables and minimizing power quality problems. The voltage source converter is one of the key elements in the power electronics field which make the significant contribution to incorporating renewables and lessening power quality problems. It is possible, due to its power conversion and power controllability features.

In this thesis, the reactive power control features in the grid-connected voltage source converter are implemented and verified through different simulations. The battery storage is used as the source of voltage during the thesis. In the implementation stage, the converter parameter and filtering technique are firstly selected, keeping in mind that the expected converter is at MW level. Later, grid synchronization and inner current control are implemented using a simple PI controller. To design the proper controller parameters, the dynamics of the converter is also analyzed. During the power control stage, conventional droop mechanism is applied to generate current reference in order to manipulate the reactive current that is generated by the converter. Manipulating the reactive current defines to what extent of reactive power is to be controlled regarding support grid voltage.

PREFACE

Firstly, I am thankful to Allah, the Almighty, who has given me a chance to come to the earth and to lead a healthy life until now. It is not enough for me to give thanks to my parents who have an uncountable contribution in my life. Then, I would like to express my sincere gratitude to the Tampere University of Technology for providing a fabulous study environment during my master of science studies. This thesis has been conducted through a lot of independent works under the guidance of Assistant Professor Tuomas Messo. So, the name Mr. Tuomas Messo comes in my mind to remember by hurt for his continuous support from the initial stage of the thesis to the end. Moreover, the word "Teach yourself " from Professor Teuvo Suntio during the lectures has worked as a tonic for me to understand something difficult independently. Special thanks go to Prof. Teuvo Suntio.

At this stage, I would like to remember and thank my relatives and friends for their co-operation toward achieving the master of science degree. My friend, Mehrdad Nahalparvari deserves special thanks for his co-operation and help during my master of science studies.

Last but not least, I would like to remember my employer company ISS palvelut oy due to its contribution to securing my livelihood. My supervisor from the workplace Sari Pesonen and her assistant Eini Hirvonen deserve special thanks.

Tampere, 19.9.2018

Md Tanjimuddin

TABLE OF CONTENTS

LIST OF FIGURES

LIST OF TABLES

LIST OF ABBREVIATIONS AND SYMBOLS

AC	Alternating Current
DC	Direct Current
FACTS	Flexible ac Transmission System
FFT	Fast Fourier Transform
GCC	Grid-Connected Converter
HVDC	High Voltage Direct Current
IEEE	Institute of Electrical and Electronics Engineers
LHP	Left Half Plane
PCC	Point of Common Coupling
P-f	Power-Frequency
PI	Proportional Integral
PLL	Phase Locked Loop
PWM	Pulse Width Modulation
Q-V	Reactive Power-Voltage
SRF-PLL	Synchronous Reference Frame-Phase Locked Loop
STATCOM	Static Compensator
VAR	Volt Ampere Reactive
VSC	Voltage Source Converter
VSI	Voltage Source Inverter

SYMBOLS

$\mathbf{A}$	Coefficient of state-space equation
$\mathbf{B}$	Coefficient of state-space equation
$\mathbf{C}$	Coefficient of state-space equation
C_f	Filter capacitor
C_b	Base capacitor
$\mathbf{D}$	Coefficient of state-space equation
D_d	Duty ratio for d-component.
D_q	Duty ratio for q-component
$\mathbf{d}$	Space vector for duty ratio
$\mathbf{d}^s$	Space vector of duty raito in synchronous reference frame
d_a	Duty ratio for a phase

d_b	Duty ratio for b phase
d_c	Duty ratio for c phase
$\mathbf{E}_c$	Generated Voltage phasor at the converter
E_c	Generated voltage at the converter
E_s	Generated voltage at the synchronous generator
E^*	Reference voltage
E	System voltage
f_{sw}	Switching frequency
f_s	Grid frequency
f_{res}	Resonant frequency
G_p	Plant transfer function
G_{PI}	PI controller transfer function
G_{SPWM}	Modulator gain
G_c	Controller transfer function
G_{ild-o}	D-channel input to converter side inductor current transfer function (open-loop)
G_{cld-o}	D-channel control to converter side inductor current transfer function (open-loop)
G_{clq-o}	Q-channel control to converter side inductor current transfer function (open-loop)
G_{cldq-o}	Cross-coupling (d-q) control to converter side inductor current transfer function (open-loop)
G_{clqd-o}	Cross-coupling (q-d) control to converter side inductor current transfer function (open-loop)
G_{ilq-o}	Q-channel input to converter side inductor current transfer function (open-loop)
G_{cid-o}	D-channel control to input transfer function (open-loop)
G_{ciq-o}	Q-channel control to input transfer function (open-loop)
G_{cod-o}	D-channel control to output transfer function (open-loop)
G_{coq-o}	Q-channel control to input transfer function (open-loop)
G_{codq-o}	Cross-coupling (d-q) control to output transfer function (open-loop)
G_{coqd-o}	Cross-coupling (q-d) control to output transfer function (open-loop)
G_{iod-o}	D-channel input to output transfer function (open-loop)
G_{ioq-o}	Q-channel input to output transfer function (open-loop)
$\boldsymbol{i}_{L1}^s$	Space vector of converter-side inductor current
$\boldsymbol{i}_{L2}^s$	Space vector of grid-side inductor current
$\boldsymbol{i}_o^s$	Space vector of output current

i_{l1a}	Current flowing through, phase a converter-side inductor
i_{l1b}	Current flowing through, phase b converter-side inductor
i_{l1c}	Current flowing through, phase c converter-side inductor
i_{l2a}	Current flowing through, phase a grid-side inductor
i_{l2b}	Current flowing through, phase b grid-side inductor
i_{l2c}	Current flowing through, phase c grid-side inductor
i_{Ca}	Current flowing through, phase a of filter capacitor
i_{Cb}	Current flowing through, phase b of filter capacitor
i_{Cc}	Current flowing through, phase c of filter capacitor
i_d	Current d-component
i_q	Current q-component
i_{oa}	Output current of phase a
i_{ob}	Output current of phase b
i_{oc}	Output current of phase c
${i_{l1q}}^*$	Converter-side inductor current reference for q channel controller
${i_{l1d}}^*$	Converter-side inductor current reference for d channel controller
i_{in}	Input current
I_{max}	Rated current
I_{l1d}	Steady-state converter-side inductor d-component
I_{l1q}	Steady-state converter-side inductor q-component
I_{l2d}	Steady-state grid-side inductor d-component
I_{l2q}	Steady-state grid-side inductor q-component
ΔI_{max}	Ripple current
I_{in}	Steady-state input current
$\mathbf{I}^{dq}$	Current phasor in dq form.
$\mathbf{I}^{\alpha\beta *}$	Current phasor conjugate dq form
k_q	Droop controller gain
K_k	PI controller gain in SRF-PLL
K_c	PI controller gain in inner current control
$k_{\alpha\beta 0}$	Clarke's transformation factor
$k_{w_s t}$	Park's transformation factor
$\mathbf{K}$	Transformation factor
L_1	Converter-side inductor
L_2	Grid-side inductor.
m	Droop coefficient for P-f droop
n	Droop coefficient for Q-V droop
P	Real power

P_n	Inverter rated active power
P^*	Reference active power
Q	Reactive power
Q^*	Reference reactive power
ΔQ_{max}	Total reactive power deviation at certain power factor
r_{L1a}	Parasitic resistance, phase a converter-side inductor
r_{L1b}	Parasitic resistance, phase b converter-side inductor
r_{L1c}	Parasitic resistance, phase c converter-side inductor
r_{L2a}	Parasitic resistance, phase a grid-side inductor
r_{L2b}	Parasitic resistance, phase b grid-side inductor
r_{L2c}	Parasitic resistance, phase c grid-side inductor
r_{eq}	Equivalence resistance
R_d	Damping resistor
S	Apparent power
T_{oid-o}	D-channel output to input transfer function (open-loop)
T_{oiq-o}	Q-channel output to input transfer function (open-loop)
T_{old-o}	D-channel output to converter-side inductor current transfer function (open-loop)
T_{olq-o}	Q-channel output to converter-side inductor current transfer function (open loop)
T_{olqd-o}	Cross-coupling (q-d) output to converter-side inductor current transfer function (open-loop)
T_{oldq-o}	Cross-coupling (d-q) output to converter-side inductor current transfer function (open-loop)
$\mathbf{U}$	Amplitude of instantenious voltage
U_{od}	Steady-state grid voltage d component
U_q	Steady-state grid voltage q component
$u_a(t)$	Instantenious phase voltage for phase a
$u_b(t)$	Instantenious phase voltage for phase b
$u_c(t)$	Instantenious phase voltage for phase c
$\mathbf{u}_{L1}$	Space vector for converter-side inductor voltage
$\mathbf{u}_{L2}$	Space vector for grid-side inductor voltage
u_{L1a}	Converter-side inductor voltage in phase a
u_{L1b}	Converter-side inductor voltage in phase b
u_{L1c}	Converter-side inductor voltage in phase c
u_{L2a}	Grid-side inductor voltage in phase a
u_{L2b}	Grid-side inductor voltage in phase b

u_{L2c}	Grid-side inductor voltage in phase c
$u_{C_f a}$	Capacitor voltage connected in phase a
$u_{C_f b}$	Capacitor voltage connected in phase b
$u_{C_f c}$	Capacitor voltage connected in phase c
u_{abc}	Three-phase voltage.
$u_{\alpha\beta 0}$	Voltage in $\alpha\beta 0$ domain
u_{dq0}	Voltage in $dq0$ domain
ΔU_{normal}	Acceptable voltage deviation
$\mathbf{U}^{\alpha\beta}$	Voltage phasor $\alpha\beta$ from
$\mathbf{U}^{dq}$	Voltage phasor dq from
U_{PCC}	Voltage at the point of common coupling
U_g	Grid voltage
U_{in}	Steady-state input voltage
U_{ph}	Phase-phase voltage.
$\mathbf{U}(s)$	Input variables in Laplace domain
u_d	Voltage d-component value
u_q	Voltage q-component value
w_{sw}	Angular switching frequency
w_s	Grid angular frequency
w^*	Reference angular frequency
w	System angular frequency
$\mathbf{x}$	Space vector
$\mathbf{x}^s$	Space vector in synchronous reference frame
X_l	Line reactance
$\mathbf{X}(s)$	State variables in laplace domain
$\mathbf{Y}(s)$	Output variables in laplace domain
Y_{in}	Input admittance (open-loop)
Y_{od-o}	D-channel output admittance (open-loop)
Y_{oq-o}	Q-channel output admittance (open-loop)
Y_{odq-o}	Cross-coupling (d-q) output admittance (open-loop)
Y_{oqd-o}	Cross-coupling (q-d) output admittance (open-loop)
Z_b	Base impedance
Z	Line impedance

Following notations used to represent differently for the same characters

$\langle\rangle$	Average value
$\widehat{\ }$	Linearized value

1. INTRODUCTION

Renewable sources are the most important energy resources which have the utmost potential to face the challenge of global warming. It would be the only viable alternative during the scarcity of fossil fuel and when the fossil fuel would completely be diminished from the earth. Utilization of renewable energy in a usable form is a prominent field of research in recent days [1]. At present, the scale of renewable energy production is low. Thus, it is prevalent that, the renewable sources are connected to the grid through the interfacing device. The power electronics converter plays a significant role as an interface between the energy source and the grid. Moreover, power transfer in an ideal form is not possible due to the intermediate interruptions of power and non-linear characteristics of the loads. On the other hand, it is necessary to supply power to the customer at the particular voltage level to meet with the operational requirements of load [2]. However, it is excellent news in the field of the power system that power electronic devices are now being used as multi-tasking purpose like, when integrating renewable into the grid it also supports the grid using its control features.

Electrical energy is generated from the power station, and it is transmitted through the transmission and distribution networks. Generally, the electrical power system is based on AC, and the simultaneous flow of both active power and reactive power is the main characteristics of the AC power system. The flow of active and reactive power happens due to the existence of several types of electrical equipment in the power system which is responsible for producing or absorbing active and reactive power. For example, synchronous machines, capacitive loads, inductive loads and transmission lines. To, distribute power to the customer level it is required to provide power with minimal losses and a fixed voltage. On the contrary, due to the nature of load and disturbances in the power system may arise voltage instability at the feeder point. One of the vital factors of voltage variation is the inability to control reactive power required by the electrical loads. Controlling reactive power from the generating station is not feasible because of the limited amount of reactive

power generating ability of generators and its associated power losses during transmission. However, the local control of reactive power can solve the issues related to the voltage instability by injecting or absorbing reactive power locally. Besides, nowadays distributed energy resources like renewable energy resources are generating electrical energy and connected to the network of distribution as well as taking part in the power-sharing process in a more flexible way.

Various types of reactive power control techniques have already been implemented to meet the requirements of local reactive power. Passive compensation is not very popular while active compensation technique is getting its popularity due to their adaptation capability with the power system dynamics [3]. In this field, power electronics is continuously emerging as a key player of reactive power compensation in power system as well as renewable energy integration due to their attractive controllability features of active and reactive power. Thyristor controlled VAR compensator is already established in the modern power system where capacitive and inductive impedance is determined by the controlling of the firing angle of thyristors. The usage of large capacitor and inductor makes the traditional VAR compensator uncomfortable to deploy in the power system due to their increased size. So, the converter based STATCOM is being developed where especially, the voltage source converter can take part in reactive power compensation and current harmonic reduction by connected in shunt with the power system. In addition to that, power electronics converters are nowadays used to incorporate renewable energy sources in the power grid. So, there is another scope of using voltage source converters to fulfill reactive power requirements at the incorporated point. In this thesis, the focus point is how reactive power is regulated in the voltage source converter and its substantial effect on keeping the voltage of the point of common coupling at permissible limits.

Several methods of reactive power control in voltage converters have been studied. Among them, conventional droop control is the most exciting and straightforward way of reactive power sharing on the local reactive power requirement. Two types of droops exist in the power system. One is frequency droop, and another one is the voltage droop. Voltage difference from the preferred level to the instantaneous level will determine the supplied or absorbed reactive power by the inverter is called voltage droop. If the voltage difference is positive, then reactive power is supplied to the point of common coupling and vice versa. Consequently, voltage droop keeps the voltage at the constant level by supplying reactive power to the grid or absorbing it from the grid [4]. The researchers in the field of power electronics have always paid

attention in the most conventional droop control method of sharing reactive power with the grid in order to meet the grid requirements.

The study process commenced through the discussion on the grid-connected converter and its application, familiarizing the theory of independent control of active and reactive power and the conventional droop method regarding control reactive power. Later, the step by step procedure is followed from the model design to the final reactive power control implementation and testing.

2. THEORY OF POWER CONTROL AND DROOP CONTROL METHOD

This chapter introduces grid-connected converter, types and its application. Nowadays more and more renewable energy sources are taking part in supplying electric power to the customer by connecting them to the grid with the help of the grid-connected converter. Conventionally, the grid-connected converter is used intending to converting electrical power one form to another depending on the end user requirement. Besides the conventional application of the grid-connected converter, this chapter describes how the grid-connected converter is used in the modern power system as a power quality enhancement device. Power quality improvement is achieved by implementing different control techniques in the converter such as DC link voltage control and the inner current control. Inner current control aids the power control of the grid-connected converter using different control methods. The droop method is used in the most of the literature, and it is classified as conventional and modified droop. Due to the limitation found using conventional droop, many researchers are proposed various droop method after the modification of conventional droop. Conventional droop regarding power control in the grid-connected converter is extensively discussed in this chapter.

2.1 Grid-connected converter

The renewable sources such as solar, wind produces electrical energy which is then transferred to the utility grid. Transferring is done by converting the produced electrical energy in a suitable form concerning frequency and forms of power (AC) for the utility grid. Moreover, power transfer from the utility grid to the load is possible through the power conversion process depending on the application. The converter which is responsible for the conversion process and made with power electronic devices is called the grid-connected converter [5, 6]. The noteworthy contribution of the grid-connected converter also in the field of flexible AC transmission system

and the HVDC transmission system [6]. The converter is in inverter mode when it converts DC power to AC power and the rectifier mode when the conversion is reversed. The Figures below interprets the grid connection of renewable sources through the grid-connected converter. Figure 2.1, showing that electrical power generated in the solar generator is DC form and delivered to the grid through the grid-connected converter by converting DC power to AC power. Despite, the wind generator in Figure 2.2, generated electrical power in AC form, the back to back connection of the converter is used to feed the generated electrical power to utility grid with appropriate frequency.

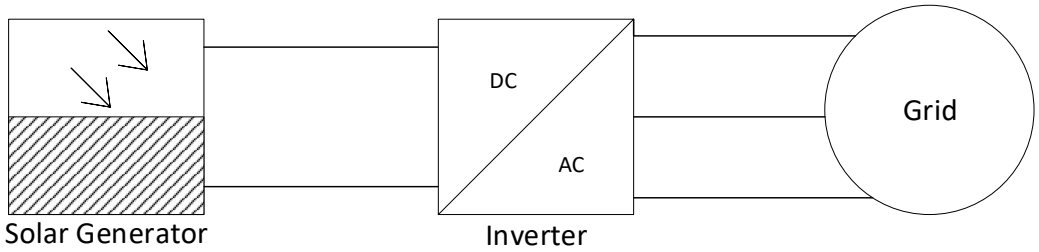

Figure 2.1 *Grid connection of solar generator*

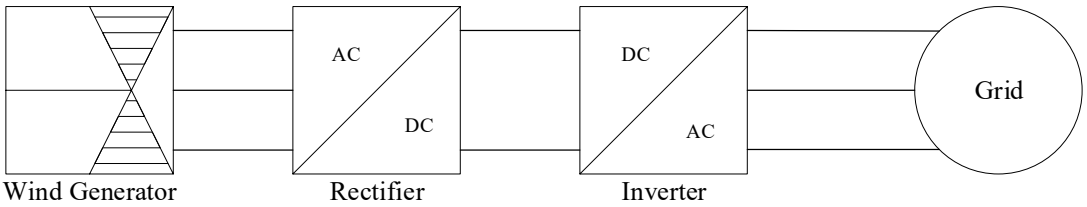

Figure 2.2 *Grid connection of wind generator*

Based on the nature of the source, the grid-connected converter can be classified in voltage and current source converter. If the source is DC voltage and unchanged during the operation of the grid converter is called a voltage source converter whereas the current source converter has an input of constant current source [7]. The example of the constant voltage source is battery storage, and the current source is the photovoltaic generator. In this thesis, the voltage source converter is chosen for the reactive power control analysis.

2.2 Applications of grid-connected converter

2.2.1 FACTS devices

Nowadays, power quality issue in the modern power system has become a significant concern. It is because of using power electronic devices, the incremental number of non-linear loads and the incorporation of renewable energy sources into the smart grid. Consequently, power system behavior is being deviated from its natural norm. During the early twenty centuries, the flexible AC transmission system evolved as a solution to power quality problems by using controllable power electronic devices as the FACTS component [8]. Power electronic device like the voltage source converter is now being taken the significant place in the field of the flexible AC transmission system.

STATCOM is a FACTS device which is mainly based on the voltage source converter usually connected in parallel with the grid to make the power system healthy. It responds very well to the power system abnormalities like voltage variation and transients. When responding with power system abnormalities, it is just using the control features of the voltage source converter. The ability of reactive power control of the voltage source converter helps to minimize voltage variation and transients at the point of interconnection [9]. STATCOM is used to generate or absorb reactive power according to the requirement when control function activates [10]. Figure 2.3 shows the simplified diagram of a STATCOM.

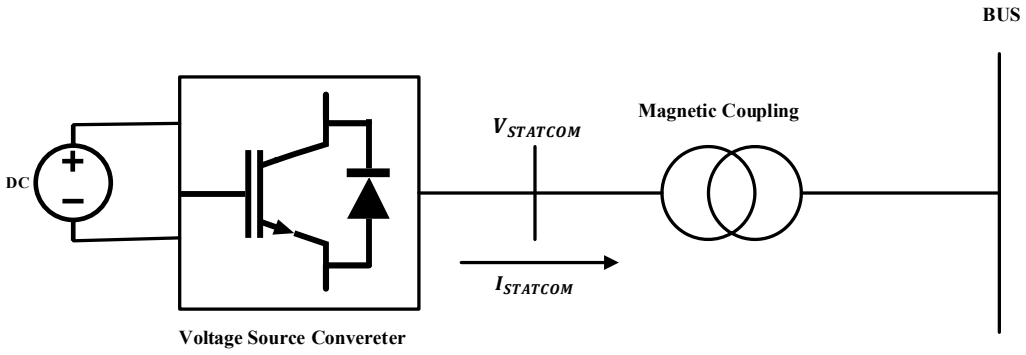

Figure 2.3 *Simplified diagram of a STATCOM connected with AC bus*

2.2.2 HVDC transmission

Traditional AC power transmission is transforming to DC transmission. Minimizing losses in long-distance transmission, the absence of synchronous and stable operation requirement, DC power transmission is getting its popularity over an AC power transmission system. Conventionally, HVDC transmission is done by the thyristor-based converter placing at sending and receiving station. Recently, the trend is to use PWM based voltage source converter as a substitution of the thyristor-based converter due to its flexible control mechanism [11]. The voltage source converter topology is made with the coupling transformer, power electronic switches, DC link capacitor, and an AC filter. The coupling transformer is used to make a magnetic coupling between AC and DC networks. The power semiconductor switches are necessary to generate the pulse using the switching mechanism. The DC link capacitor preserves DC voltage into it and takes part to minimize switching transients and harmonics. Finally, AC filter is used to reduce harmonic's that is produced at the converter output to improve the power quality of converting power [12].

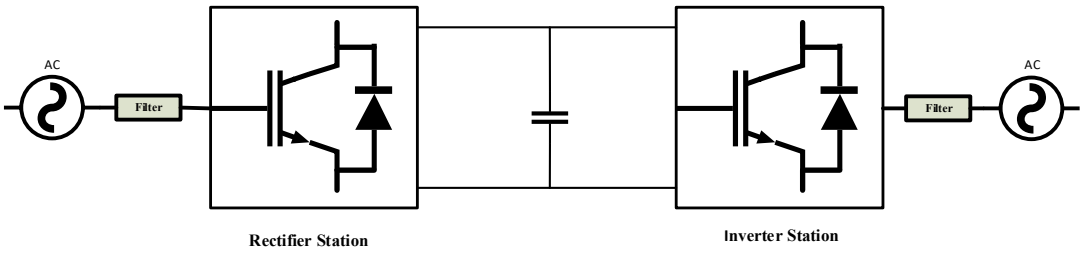

Figure 2.4 *Simplified diagram of a VSC based HVDC transmission*

2.2.3 Microgrid

A group of electrically connected substance which makes a small electrical network is called microgrid. Electrical substances, for example, distributed energy like renewable energy sources, storage devices, various types of load. A microgrid can operate either as an islanded mode or in synchronism with the smart grid. In a microgrid, distributed generators like solar, wind, battery storages, fuel cells are connected through the grid-connected converter. The grid-connected converter does not only

serve as an interface in microgrid it also utilizes its control facilities. According to the control facilities, the grid-connected converter can be classified into grid-feeding, grid-forming and grid-supporting grid-connected converter. Furthermore, depending on the source used in the grid support converter it can be classified as grid-support grid-feeding and grid-support grid-forming. Four types of the grid-connected converter used in the microgrid are discussed subsequently.

1. **Grid-forming grid-connected converter**: If a grid-connected converter, is acting as a voltage source to produce constant voltage and frequency at its output then the term grid-forming is used to identify the type of the converter. It is possible when there is only one source available and forming a grid with one central inverter. Voltage control loop is used to regulate the voltage according to the grid voltage [13].

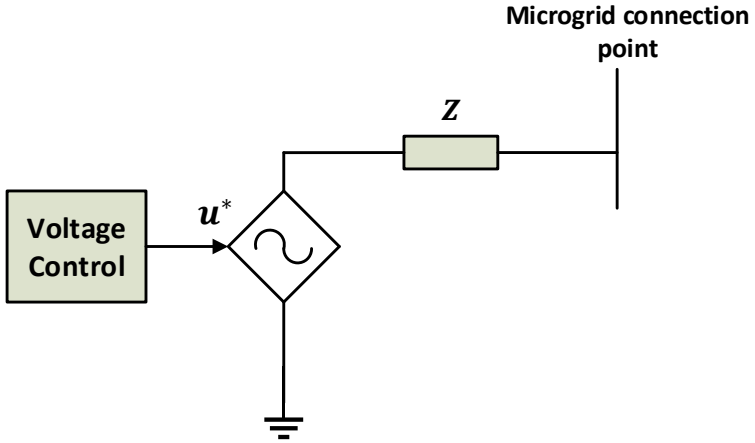

Figure 2.5 *Grid-forming inverter*

2. **Grid-feeding grid-connected converter**: The term grid-feeding is applied when there are multiple sources are available in the grid and those sources are acting as a current source and feeding power to the grid. This scenario exists in a microgrid where there is many sources are connected to form a microgrid. This microgrid is operated in grid-connected mode. The power control loop is required to regulate active and reactive power to the grid [13].

3. **Grid supporting grid-connected converter**: The grid supporting converter is used to control their output current or voltage to keep the energized

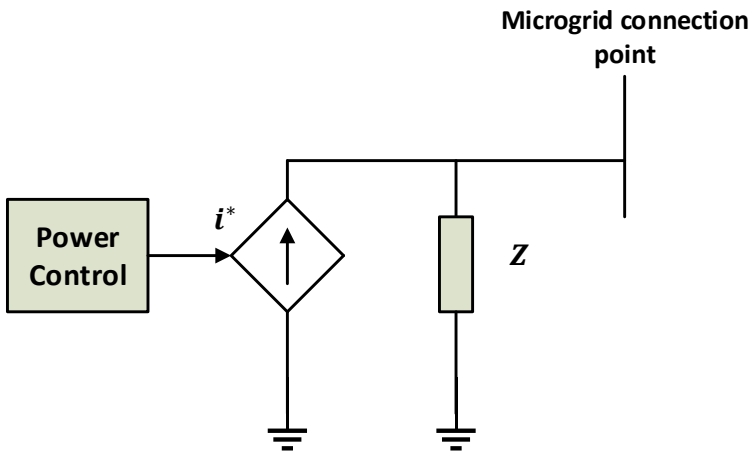

Figure 2.6 *Grid-feeding inverter*

grid at defined voltage and frequency. Thus, this grid support grid-connected converter operated at either as a current source or a voltage source. Depending on the used source type, to form grid support grid-connected converter can be categorized as grid support grid feeding and grid support grid forming.

(a) **Grid-support grid-forming**: In this type of grid converter, power is controlled according to the AC grid voltage expressing its characteristics as an AC voltage source. It is connected to the grid through virtual or physical link impedance. The grid support grid forming converter can adjust grid voltage and frequency according to the power level of the converter. Figure 2.7, represents the grid-support grid-forming converter where power is transferred to the grid according to AC grid voltage [13].

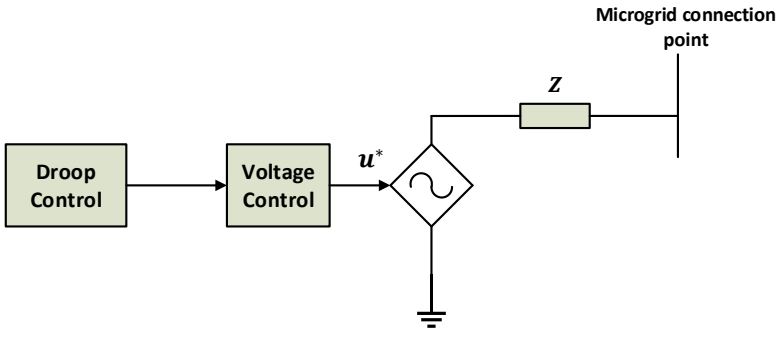

Figure 2.7 *Grid-support grid-forming inverter*

(b) **Grid-support grid-feeding**: Power is delivered to the load forming a grid-feeding converter. The grid-support is additionally done in grid-support grid-feeding converter by contributing in preserving the defined grid voltage and frequency. The main purpose of regulating grid frequency and voltage is done by the power converter acting as a current source. The power converter is connected to the grid with parallel high impedance. Figure 2.8, shows the simplified diagram of a grid-support grid-feeding [13].

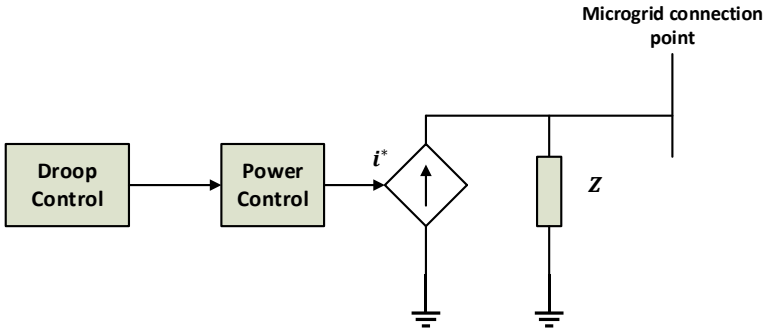

Figure 2.8 *Grid-support grid-feeding inverter*

2.3 Power control theory

Conventionally, the power system comprises three-phase voltages and currents in sinusoidal form. The time-varying nature and their sinusoidal components make the power calculation complex. To avoid this complexity, three-phase voltages and currents can be first, transformed into $\alpha\beta 0$ stationary reference frame, where three-phase components are designated as α, β and zero components. If the power system is balanced, the zero component can be neglected to make the calculation easy. Nevertheless , α and β components are still oscillating in nature, which makes the designing of conventional PI controller in $\alpha\beta$ frame is difficult. The accurate design of a PI controller requires to have the controller input quantities in DC form. according to this requirement, $\alpha\beta 0$ stationary reference frame then transformed into synchronously rotating reference frame. Transforming three-phase quantities to $\alpha\beta 0$ quantities is called Clarke's transformation whereas transforming $\alpha\beta 0$ to dq0 is called Park's transformation. The process considering amplitude invariant transformation is described as follows.

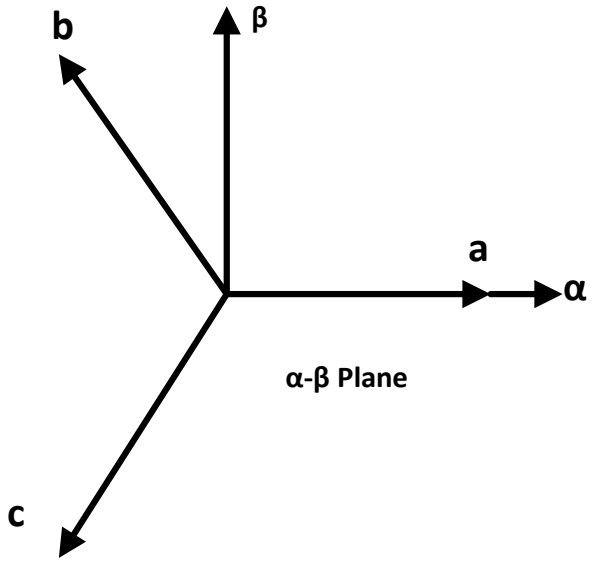

Figure 2.9 *Stationary reference frame*

2.3.1 Clarke's transformation

The transformation is used to obtain α,β, and 0 component from the three-phase variable is called Clarke's transformation. [14]. Transfromation and the reverse transformations of three-phase voltages and currents are given in equation. It is noted that if three-phase system is balanced then, zero components of $\alpha\beta 0$ can be neglected.

$$\left[u_{\alpha\beta 0}\right] = \left[K_{\alpha\beta 0}\right]\left[u_{abc}\right] \tag{2.1}$$

$$\left[i_{abc}\right] = \left[K_{\alpha\beta 0}\right]^{-1}\left[i_{\alpha\beta 0}\right] \tag{2.2}$$

Where, $\left[K_{\alpha\beta 0}\right]$, $\left[K_{\alpha\beta 0}\right]^{-1}$ are the transformation and reverse transformation factor respectively. Their values have been found in [14] and are given in below.

$$\left[K_{\alpha\beta 0}\right] = \frac{2}{3}\begin{bmatrix} 1 & -\frac{1}{2} & -\frac{1}{2} \\ 0 & \frac{\sqrt{3}}{2} & -\frac{\sqrt{3}}{2} \\ \frac{1}{2} & \frac{1}{2} & \frac{1}{2} \end{bmatrix} \tag{2.3}$$

$$\left[K_{\alpha\beta 0}\right]^{-1} = \begin{bmatrix} 1 & 0 & 1 \\ -\frac{1}{2} & \frac{\sqrt{3}}{2} & 1 \\ -\frac{1}{2} & -\frac{\sqrt{3}}{2} & 1 \end{bmatrix} \tag{2.4}$$

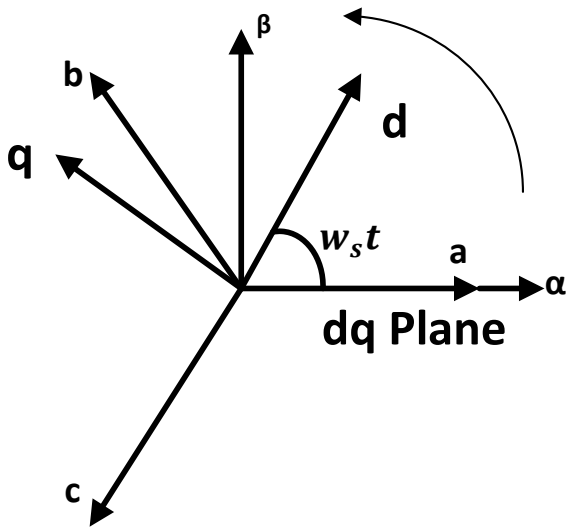

Figure 2.10 *Synchronous reference frame*

2.3.2 Park's transformation

A rotational frame which rotates with the synchronous speed with the system is called the rotating reference frame. The transformation of the rotational reference frame from the stationary reference is obtained using a method called Park's transformation method. The transformed quantities in the rotational frame are designated as direct (d), quadrature (q) and zero components. Transformation into rotating reference from $\alpha\beta 0$ frame is given in equation (2.5).

$$\left[u_{dq0}\right] = \left[K_{dq0}\right]\left[u_{\alpha\beta 0}\right] \tag{2.5}$$

$$\left[i_{dq0}\right] = \left[K_{dq0}\right]\left[i_{\alpha\beta 0}\right] \tag{2.6}$$

Where, $\left[K_{dq0}\right]$ is the transformation factor. Their values have been found in [14, 15] and is given in below.

$$\left[K_{dq0}\right] = \begin{bmatrix} \cos(w_s t) & \sin(w_s t) & 0 \\ -\sin(w_s t) & \cos(w_s t) & 0 \\ 0 & 0 & 1 \end{bmatrix} \tag{2.7}$$

2.3.3 Direct dq0 transformation from three-phase variables

Direct transformation into dq0 from three-phase variables is resulted by combining Clarke's and Park's transformation together.

$$\left[u_{dq0}\right] = \left[K_{w_s t}\right]\left[u_{abc}\right] \tag{2.8}$$

The factor of transformation is formed by combinning $\left[K_{\alpha\beta 0}\right]$ $\left[K_{dq0}\right]$ and is given below

$$\left[K_{w_s t}\right] = \frac{2}{3}\begin{bmatrix} \cos(w_s t) & \cos(w_s t - \frac{2\pi}{3}) & \cos(w_s t - \frac{4\pi}{3}) \\ -\sin(w_s t) & -\sin(w_s t - \frac{2\pi}{3}) & -\sin(w_s t - \frac{4\pi}{3}) \\ \frac{1}{2} & \frac{1}{2} & \frac{1}{2} \end{bmatrix} \tag{2.9}$$

2.3.4 Power equation of three-phase system in stationary frame

The representation of voltages and currents of three-phase system is the following

$$\begin{aligned} u_a(t) &= \sqrt{2}U\cos(w_s t + \theta) \\ u_b(t) &= \sqrt{2}U\cos(w_s t + \theta - \frac{2\pi}{3}) \\ u_c(t) &= \sqrt{2}U\cos(w_s t + \theta + \frac{2\pi}{3}) \end{aligned} \tag{2.10}$$

Current equations in three-phase system in instantaneous form is similar to the equation (2.10). α,β, and 0 components are given below after transformation according to the equation (2.1)

$$\begin{aligned} u_\alpha &= \sqrt{2}U\cos(w_s t + \theta) \\ u_\beta &= -\sqrt{2}U\sin(w_s t + \theta) \\ u_0 &= 0 \end{aligned} \tag{2.11}$$

The current equation in stationary frame after transformation is similar to the equation (2.11). Current and voltage phasors can be written in the following form.

$$\mathbf{U}^{\alpha\beta} = \frac{u_\alpha - j u_\beta}{\sqrt{2}} \tag{2.12}$$

$$\mathbf{I}^{\alpha\beta} = \frac{u_\alpha - j i_\beta}{\sqrt{2}} \tag{2.13}$$

three-phase power in $\alpha\beta$ frame can be obtained from the following equation

$$S = P + jQ = 3\mathbf{U}^{\alpha\beta}\mathbf{I}^{\alpha\beta *} = 3(\frac{u_\alpha - ju_\beta}{\sqrt{2}})(\frac{i_\alpha + ji_\beta}{\sqrt{2}}) \tag{2.14}$$

active and reactive power can be expressed as follows

$$P = \frac{3}{2}(u_\alpha i_\alpha + u_\beta i_\beta) \tag{2.15}$$

$$Q = \frac{3}{2}(u_\alpha i_\beta - u_\beta i_\alpha) \tag{2.16}$$

2.3.5 Power equation of three-phase system in synchronous reference frame

To get the constant values to form the sinusoidally oscillating variables, it can be considered that the synchronous reference frame is rotating at w_s angular frequency. Equation (2.17) shows that conversion from stationary to the rotational synchronous reference

$$\left[u_{dq}\right] = \begin{bmatrix} \cos(w_s t) & \sin(w_s t) \\ -\sin(w_s t) & \cos(w_s t) \end{bmatrix} \left[u_{\alpha\beta}\right] \tag{2.17}$$

Thus, representation of voltage and current phasors in dq domain can be witten similary as $\alpha\beta$ domain and given in equatiom (2.18) and (2.19)

$$\mathbf{U}^{dq} = \frac{u_d - ju_q}{\sqrt{2}} \tag{2.18}$$

$$\mathbf{I}^{dq} = \frac{i_d - ji_q}{\sqrt{2}} \tag{2.19}$$

three-phase power in dq frame can be obtained from the following equation

$$S = P + jQ = 3\mathbf{U}^{dq}\mathbf{I}^{dq *} = 3(\frac{u_d - ju_q}{\sqrt{2}})(\frac{i_d + ji_q}{\sqrt{2}}) \tag{2.20}$$

active and reactive power can be expressed as follows

$$P = \frac{3}{2}(u_d i_q + u_d i_q) \tag{2.21}$$

$$Q = \frac{3}{2}(u_d i_q - u_d i_q) \tag{2.22}$$

2.3.6 Current reference generation

When the grid-connected converter is synchronized with the grid, generally the q component of grid voltage and converter voltage is zero. The synchronization process is described in the next chapter. Thus, the power equation can be re-write in the following equations (2.23) and (2.24).

$$P = \frac{3}{2}(u_d i_d) \tag{2.23}$$

$$Q = \frac{3}{2}(-u_d i_q) \tag{2.24}$$

Controlling active and reactive power is possible if an accurate current reference is generated according to power theory in dq frame [16], for the PI controller. The PI controller is used to controlling the inner current in the converter by comparing the real current flowing through the converter and the reference current. The change of reference current means the converter is actively controlling its power according to the requirement. Suppose, P^* amount of active power control is desired and the corresponding reference for d component current is given in equation (2.25).

$${i_d}^* = \frac{2}{3}\frac{P^*}{u_d} \tag{2.25}$$

When Q^* amount of reactive power control is desired and corresponding reference for q component current is given in equation (2.26).

$${i_q}^* = -\frac{2}{3}\frac{Q^*}{u_d} \tag{2.26}$$

The power controller (active and reactive) is required, in order to generate the current reference. The control strategy used in power controller is described in the following sections. The converter rating determines the boundary for reference generation. Reactive power control affects supplying active power to the point of common coupling and vice -versa.

2.4 Droop control strategy

The reactive power regulation in the grid-connected converter, with respect to the voltage level at the point of interconnection, is the promising technique used in minimizing power quality problems at the PCC. The power quality problems like voltage

sags or swells can be minimized by supplying or absorbing the reactive power respectively. The regulation of power (active and reactive) in the grid-connected converter can be made as control strategies used to control frequency and excitation in the synchronous generator[17, 18, 19, 20]. In a synchronous generator, droop control mechanism is used. Advantages like independent power control, simple control algorithm, and the significant level of power controlling accuracy made the droop control famous for the power control in the grid-connected converter[21, 22]. In reactive power control conventionally Q-V droop and active power control, P-f droop is used. Active and reactive power transfer equation to the grid from a synchronous generator is given below according to Figure 2.11 [23].

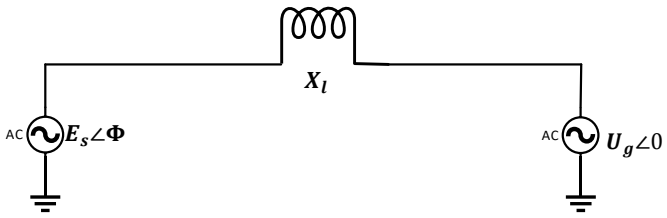

Figure 2.11 *Single line diagram of synchronous generator connected to the grid*

$$P_s = \frac{E_s U_g}{X_l} \sin\phi \tag{2.27}$$

$$\begin{aligned} Q_s &= \frac{E_s U_g \cos\phi - {U_g}^2}{X_l} \\ &= \frac{U_g}{X_l}(E_s \cos\phi - U_g) \\ &= \frac{U_g}{X_l}(E_s - U_g) \quad [When, \cos\phi = 1] \end{aligned} \tag{2.28}$$

Where, P_s, Q_s denoted as active and reactive power transfer respectively. E_s and U_g are the generated voltage at the synchronous generator and grid voltage respectively. X_l is the coupling inductance. According to the equation (2.27), it is apparent active power depends on the frequency of the generator and similarly equation (2.28) represents reactive power depends on the amplitude of the voltage difference concerning sending and receiving end voltage. Thus, active power-frequency and reactive power-voltage amplitude curve can be drawn in the following Figure 2.12. The characteristics curve represented in Figure 2.12 employs two linear equations given in (2.29 - 2.30).

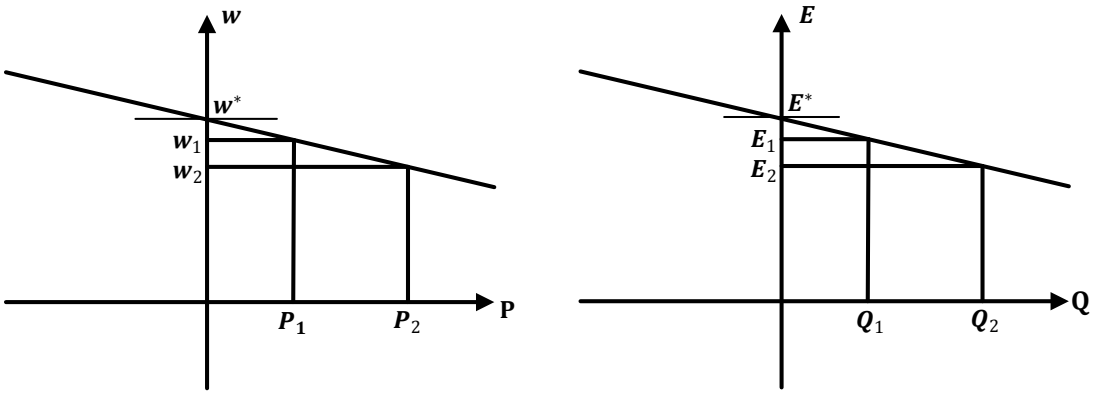

Figure 2.12 *P-f and Q-V droop characteristics*

$$w = w^* - m(P - P^*) \tag{2.29}$$

$$E = E^* - n(Q - Q^*) \tag{2.30}$$

Where,

w = system angular frequency;

P^*=reference active power;

w^*= reference angular frequency;

P = active power;

E^*=reference voltage;

E= system Voltage;

Q^*=reference reactive power;

Q= reactive power;

m= droop coefficient for active power frequency droop;

n=droop coefficient for reactive power voltage droop.

This droop characteristic can also be implemented in inverter reactive power control by designing an outer control loop. This is illustrated in the Figure 2.13. The design of droop control is described in chapter 4.

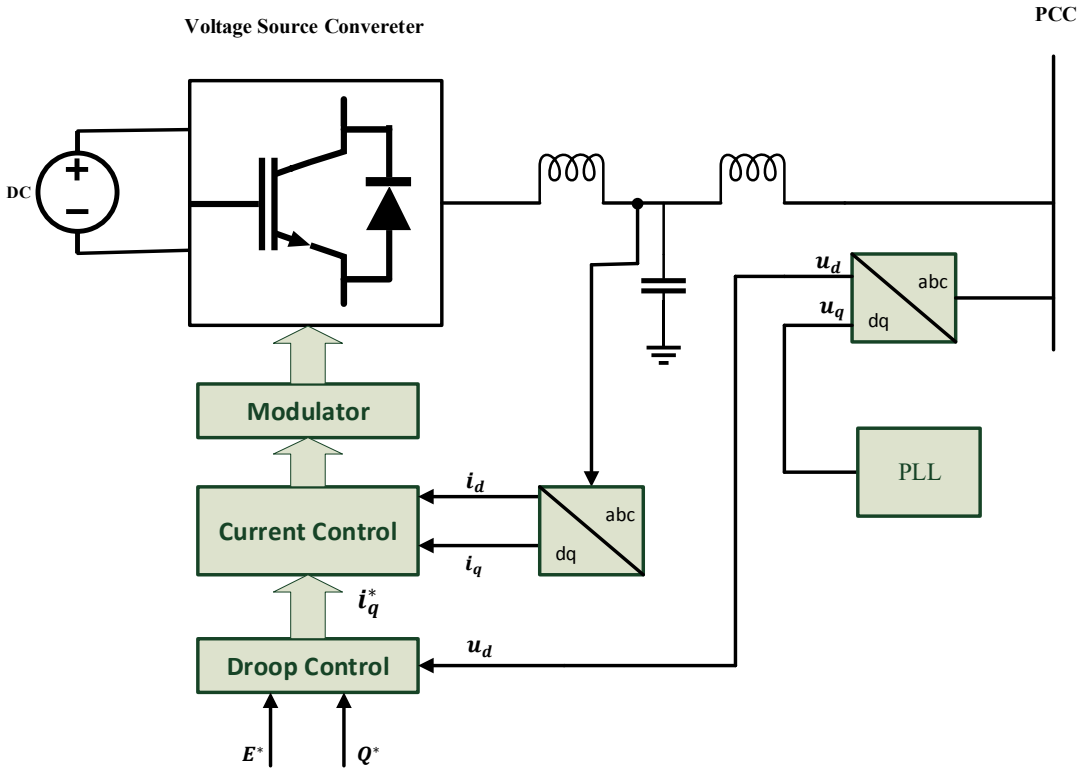

Figure 2.13 *Reactive power droop control structure*

3. DESIGN PARAMETER SELECTION OF MW LEVEL CONVERTER AND ITS DYNAMIC MODELING

This chapter presents the design parameter selection of VSI based, two level, three-phase grid-connected inverter. The summary of the designed inverter specification is given in Table 3.1. The grid-connected inverter is equipped with a filtering technique at its output, called LCL filtering. The selection procedure of filter parameters is another scope of this chapter. Subsequently, the inverter dynamic modeling is performed to derive the input-output transfer function of related inverter parameters in order to control reactive power. It is noted here is that source and load effect in the performed dynamic analysis is not presented. Such type of derived dynamic model is known as unterminated model [24, 25]. In addition to that, the effect of the control function is not discussed as well in this chapter.

To ensure high power quality from the inverter, a low pass filter is necessary to be used between the inverter and coupling point of the grid. Different types of filtering techniques are used to supply quality power to the grid. Among them, L, LC and LCL filter is researched in numerous research articles. In this thesis, LCL filter is used due to, reduced inductor size, higher power handling capacity and higher attenuation capacity of switching harmonics [26, 27, 28, 29]. However, it is also found in the literature that, introducing LCL filter has some worth noting drawbacks such as additional resonance peaking, limiting the current control bandwidth and complicated dynamic response [26, 27, 28, 29]. A damping method is used to overcome the considerable problems associated with LCL filtering. Active or passive damping is used in this regard. Damping is called passive when a resistor is connected with the inductor or capacitor either in series or parallel whereas active damping includes some extra control algorithms [29]. For the simplicity and to avoid the complexity of adding a control mechanism, the passive method of damping is used in this research. Figure 3.1 illustrates the grid-connected converter equipped with an LCL filter. The

parasitic elements of inductors and capacitor are also included in this figure.

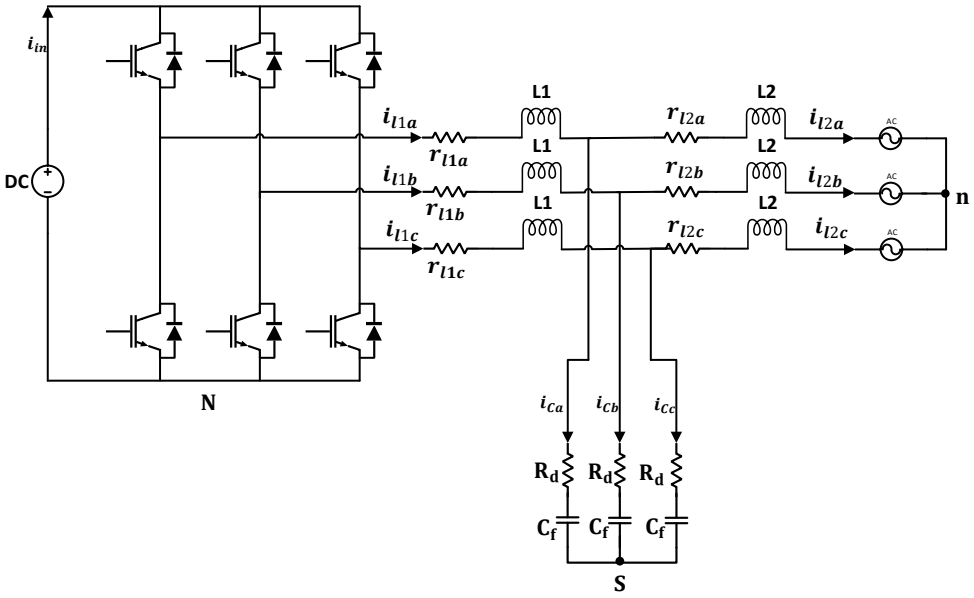

Figure 3.1 *Grid-connected converter with LCL filter*

Table 3.1 *Inverter Specification*

1	**Sytem size**	**1001.25 KVA**
2	**Inverter architecture**	**Two-level, three-phase**
3	**Inverter active power rating,P_n**	**1 MW**
4	**Line-line voltage, E_n**	**690 V**
5	**DC bus voltage, U_{DC}**	**2500 V**
7	**Minimum reactive power capacity**	**50 KVAr**
8	**IGBT voltage rating**	**4.5 KV**
9	**Power factor**	± 0.99 **to** ± 0.85

3.1 Design of LCL filter

The filter parameter is selected based on some specifications of the grid-connected converter such as converter power capacity, the frequency of the grid and switching frequency of the converter aiming to lower harmonics at the converter output [30]. To choose proper filter parameters, many works of literature is studied. Based on the references [30, 31, 32, 33, 34] the procedure of selecting inductor both for the grid and converter side, capacitor and resistor which is used to damp the resonance caused by LCL filter are discussed in the following sections, and calculated values are presented in Table 3.2.

3.1.1 Inverter side inductance calculation

Inverter side inductor sizing depends on the permitted ripple current through the inductor. The amount of ripple current also determines switching losses and conduction losses. If the ripple current is small, conduction and switching losses are low. However, a low amount of ripple increases the size of the inductor and consequently increases the core loss in the inductor. In this LCL filter design, allowed ripple current through the inductor is 10% of the rated current. For the sizing of the inverter side inductor, equation (3.1-3.3) found in [30, 31, 32, 33, 34] is used.

$$I_{max} = \frac{P_n\sqrt{2}}{3U_{ph}} \tag{3.1}$$

Ripple current through the inductor is given by

$$\Delta I_{Lmax} = 0.1 I_{max} \tag{3.2}$$

Inverter side inductor is given by

$$L_1 = \frac{V_{DC}}{6 f_{sw} \Delta I_{Lmax}} \tag{3.3}$$

3.1.2 Filter capacitor design

Reactive power flowing through the capacitor is the main tradeoff in designing filter capacitor. Higher capacitance draws a high amount of reactive power which then

demands a high amount of current from the inverter side inductor. As a result, the efficiency of the inverter is negatively affected. On the other hand, the capacitance cannot be too small in order to meet the harmonic attenuation requirements. Moreover, small capacitance results in larger inductance which is the cause of increased voltage drops across the inductor. It is found in [32] that, usually reactive power variation of 5% is taken into account in designing filter capacitance. The following formulas are used to find the value of the capacitor in LCL filter design [30, 31, 32, 33, 34].
The base value of the capacitor is defined by the equation

$$C_b = \frac{1}{w_s Z_b} \tag{3.4}$$

Where,

$$Z_b = \frac{E_n^2}{P_n} \tag{3.5}$$

Filter capacitance is given by

$$C_f = 0.05 C_b \tag{3.6}$$

3.1.3 Grid side inductor design

The injected harmonic current to the grid is the factor affecting the sizing of the inductor connected to the grid, after the sizing of the inductor on the inverter side and the filter capacitor. In this thesis 20% harmonics generated on the inverter side is attenuated before injecting the current to the grid is taken. The formula found in [32] is used to determine grid side inductance.

$$L_2 = \frac{\sqrt{\frac{1}{K_a^2}} + 1}{C_f w_{sw}^2} \tag{3.7}$$

3.1.4 Resonant frequency and passive damping

To avoid resonance in the resonance frequency band following condition (3.9) should be satisfied. Passive damping is used to avoid resonance caused by LCL filter as well. The resonance frequency of the LCL filter is given by the equation (3.8).

$$w_{res} = \sqrt{\frac{L_1 + L_2}{L_1 L_2 C_f}} \tag{3.8}$$

Table 3.2 *LCL filter parameters*

f_s	Grid frequency	50 Hz
f_{sw}	Switching frequency	5 KHz
P_t	Rated active power	1 MW
V_{ph}	Phase grid voltage	398.37 V
L_1	Inductor, Inverter-side	704 μH
L_2	Inductor, Grid-side	20 μH
C_f	Filter capacitor	300 μF
R_d	Damping resistor	0.015 Ω

$$10f_s < f_{res} < 0.5f_{sw} \tag{3.9}$$

Value of the passive resistor in order to damp the resonance is given by the equation (3.10)

$$R_d = \frac{1}{3w_{res}C_f} \tag{3.10}$$

3.2 Average modeling

The synchronous reference frame is used to model the three-phase two-level inverter for small signal analysis. The reference frame is assumed to rotate at grid angular frequency and transforms three-phase phase variable in ordinary reference frames to the synchronous reference frame. As a result, three-phase sinusoidal voltage and currents are converted to dc valued signal. It is convenient to solve the steady-state operating points and linearize the average model in the synchronous reference frame, and its associated converted dc valued components. Three components of rotating space vector named as alpha, beta and zero are used to represent the three-phase system. Equation (3.11) and (3.12) depicts the complex and real-valued representation of the space vector of a three-phase system. Scaling factor K depends on the type of transformation. When the transformation is amplitude invariant, the scaling factor is $\frac{3}{2}$, and scaling factor $\sqrt{\frac{3}{2}}$ is used during the power invariant transformation. In this thesis, amplitude invariant transformation is used.

$$\boldsymbol{x} = x_\alpha + jx_\beta = \boldsymbol{K}(x_a + x_b e^{\frac{j2\pi}{3}} + x_c e^{\frac{j4\pi}{3}}) \tag{3.11}$$

$$x_0 = \frac{x_a + x_b + x_c}{3} \tag{3.12}$$

The average voltage across the inductor and currents through the capacitor is derived using Kirchhoff's voltage and current law for small signal modeling. The averaging is done in one complete switching cycle based on Figure 3.1. The resistance r_{eq}, is used to represent on-time switching resistance and parasitic resistance of the inverter side inductance in each phase.

$$\langle u_{L1a}\rangle = d_A\langle u_{in}\rangle - (r_{eq}+R_d)\langle i_{l1a}\rangle - \langle u_{C_fa}\rangle + R_d\langle i_{l2a}\rangle - \langle u_{SN}\rangle \tag{3.13}$$

$$\langle u_{L2a}\rangle = -(r_{l2a}+R_d)\langle i_{l2a}\rangle + R_d\langle i_{l1a}\rangle - \langle u_{an}\rangle + \langle u_{Sn}\rangle + \langle u_{C_fa}\rangle \tag{3.14}$$

$$\langle u_{L1b}\rangle = d_B\langle u_{in}\rangle - (r_{eq}+R_d)\langle i_{l1b}\rangle - \langle u_{C_fb}\rangle + R_d\langle i_{l2b}\rangle - \langle u_{SN}\rangle \tag{3.15}$$

$$\langle u_{L2b}\rangle = -(r_{l2b}+R_d)\langle i_{l2b}\rangle + R_d\langle i_{l1b}\rangle - \langle u_{bn}\rangle + \langle u_{Sn}\rangle + \langle u_{C_fb}\rangle \tag{3.16}$$

$$\langle u_{L1c}\rangle = d_C\langle u_{in}\rangle - (r_{eq}+R_d)\langle i_{l1c}\rangle - \langle u_{C_fc}\rangle + R_d\langle i_{l2c}\rangle - \langle u_{SN}\rangle \tag{3.17}$$

$$\langle u_{L2c}\rangle = -(r_{l2c}+R_d)\langle i_{l2c}\rangle + R_d\langle i_{l1c}\rangle - \langle u_{cn}\rangle + \langle u_{Sn}\rangle + \langle u_{C_fc}\rangle \tag{3.18}$$

$$\langle i_{Ca}\rangle = \langle i_{l1a}\rangle - \langle i_{l2a}\rangle \tag{3.19}$$

$$\langle i_{Cb}\rangle = \langle i_{l1b}\rangle - \langle i_{l2b}\rangle \tag{3.20}$$

$$\langle i_{Cc}\rangle = \langle i_{l1c}\rangle - \langle i_{l2c}\rangle \tag{3.21}$$

$$\langle i_{oa}\rangle = \langle i_{l2a}\rangle \tag{3.22}$$

$$\langle i_{ob}\rangle = \langle i_{l2b}\rangle \tag{3.23}$$

$$\langle i_{oc}\rangle = \langle i_{l2c}\rangle \tag{3.24}$$

$$\langle i_{in}\rangle = d_A\langle i_{l1a}\rangle + d_B\langle i_{l1b}\rangle + d_c\langle i_{l1c}\rangle \tag{3.25}$$

The average inductor voltage and currents equation can be represented in space vectors given in

$$\langle \boldsymbol{u}_{L1}\rangle = \boldsymbol{d}\langle u_{in}\rangle - (r_{eq}+R_d)\langle \boldsymbol{i}_{l1}\rangle - \langle \boldsymbol{u}_{C_f}\rangle + R_d\langle \boldsymbol{i}_{l2}\rangle \tag{3.26}$$

$$\langle \boldsymbol{u}_{L2}\rangle = -(r_{l2}+R_d)\langle \boldsymbol{i}_{l2}\rangle + R_d\langle \boldsymbol{i}_{l1}\rangle + \langle \boldsymbol{u}_{C_f}\rangle - \langle \boldsymbol{u}_0\rangle \tag{3.27}$$

$$\langle \boldsymbol{i}_C\rangle = \langle \boldsymbol{i}_{l1}\rangle - \langle \boldsymbol{i}_{l2}\rangle \tag{3.28}$$

$$\langle \boldsymbol{i}_o\rangle = \langle \boldsymbol{i}_{l2}\rangle \tag{3.29}$$

Where,
$\langle \boldsymbol{u}_{L1}\rangle = \frac{2}{3}(\langle u_{L1a}\rangle e^{j0} + \langle u_{L1b}\rangle e^{\frac{j2\pi}{3}} + \langle u_{L1c}\rangle e^{\frac{j4\pi}{3}})$

$\langle \boldsymbol{d} \rangle = \frac{2}{3}\big(\langle d_A \rangle e^{j0} + \langle d_B \rangle e^{\frac{j2\pi}{3}} + \langle d_C \rangle e^{\frac{j4\pi}{3}}\big)$
$\langle \boldsymbol{u}_{L2} \rangle = \frac{2}{3}(\langle u_{L2a} \rangle e^{j0} + \langle u_{L2b} \rangle e^{\frac{j2\pi}{3}} + \langle u_{L2c} \rangle e^{\frac{j4\pi}{3}})$
$\langle \boldsymbol{i}_{l1} \rangle = \frac{2}{3}(\langle i_{l1a} \rangle e^{j0} + \langle i_{l1b} \rangle e^{\frac{j2\pi}{3}} + \langle i_{l1c} \rangle e^{\frac{j4\pi}{3}})$
$\langle \boldsymbol{i}_{l2} \rangle = \frac{2}{3}(\langle i_{l2a} \rangle e^{j0} + \langle i_{l2b} \rangle e^{\frac{j2\pi}{3}} + \langle i_{l2c} \rangle e^{\frac{j4\pi}{3}})$
$\langle \boldsymbol{i}_{0} \rangle = \frac{2}{3}(\langle i_{oa} \rangle e^{j0} + \langle i_{ob} \rangle e^{\frac{j2\pi}{3}} + \langle i_{oc} \rangle e^{\frac{j4\pi}{3}})$
$\langle \boldsymbol{u}_{c_f} \rangle = \frac{2}{3}(\langle u_{C_f a} \rangle e^{j0} + \langle u_{C_f b} \rangle e^{\frac{j2\pi}{3}} + \langle u_{C_f c} \rangle e^{\frac{j4\pi}{3}})$
$\langle \boldsymbol{u}_{o} \rangle = \frac{2}{3}(\langle u_{an} \rangle e^{j0} + \langle u_{bn} \rangle e^{\frac{j2\pi}{3}} + \langle u_{cn} \rangle e^{\frac{j4\pi}{3}})$

$\langle \boldsymbol{u}_{L1} \rangle$,$\langle \boldsymbol{i}_{l1} \rangle$,$\langle \boldsymbol{u}_{L2} \rangle$,$\langle \boldsymbol{i}_{l2} \rangle$, $\langle \boldsymbol{i}_{0} \rangle$, $\langle \boldsymbol{d} \rangle$,$\langle \boldsymbol{u}_{C_f} \rangle$,$\langle \boldsymbol{u}_{o} \rangle$ represents the rotating space vectors of inductor voltage and currents with respect to inverter side, inductor voltage and currents for grid side, converter output current, duty ratio, filter capacitor voltage and output voltage.$\langle \boldsymbol{i}_{C} \rangle$ is the grid capacitor current.

Using the synchronous reference frame instead of the stationary reference frame is convenient and easy in regard to solving operating points in the steady-state and linearization of the converter at the solved operating points. Moreover, in a synchronous reference frame, AC quantities converted to DC values which makes the possibility of using the conventional PI controller [35, 36, 37]. However, the cross-coupling effect introduced in the synchronous reference frame which is then eliminated by using decoupling gains. In this thesis, the synchronous reference frame is used to analyze the dynamics of the inverter. The Park's transformation is used during the process of stationary to synchronous conversion. The space vectors in a synchronous frame are symbolized as direct (d), quadrature (q) and zero (o). Park's transformation is given in equation (3.30).

$$\mathbf{x}_s = \mathbf{x} e^{-jw_s t} = x_d + j x_q \tag{3.30}$$

Following equations are obtained by converting equations (3.26)-(3.29) into synchronous reference frame by using (3.30)

$$\frac{d\langle \boldsymbol{i}^s_{l1} \rangle}{dt} = \frac{1}{L_1}\big[\boldsymbol{d}^s \langle u_{in} \rangle - (r_{eq} + R_d + j w_s L_l)\langle \boldsymbol{i}^s_{l1} \rangle + R_d \langle \boldsymbol{i}^s_{l2} \rangle - \langle \mathbf{u}^s_{C_f} \rangle\big] \tag{3.31}$$

$$\frac{d\langle \boldsymbol{i}^s_{l2} \rangle}{dt} = \frac{1}{L_2}\big[- (r_{l2} + R_d + j w_s L_2)\langle \boldsymbol{i}^s_{l2} \rangle + R_d \langle \boldsymbol{i}^s_{l1} \rangle + \langle \boldsymbol{u}^s_{C_f} \rangle - \langle \boldsymbol{u}^s_{o} \rangle\big] \tag{3.32}$$

Output capacitor current can be expressed as the time derivative of the capacitor

voltage and converting it to synchronous reference frame as given in equation (3.33)

$$\frac{d\langle \boldsymbol{u}^s_{C_f}\rangle}{dt} = \frac{1}{C_f}\big[\langle \boldsymbol{i}^s_{l1}\rangle - \langle \boldsymbol{i}^s_{l2}\rangle - jw_sC_f\langle \boldsymbol{u}^s_{C_f}\rangle\big] \tag{3.33}$$

$$\langle \boldsymbol{i}^s_o\rangle = \langle \boldsymbol{i}^s_{l2}\rangle \tag{3.34}$$

input current of equation (3.25) can be transformed in dq domain by using inverse Park's transformation and given in equation (3.35)

$$\langle i_{in}\rangle = \frac{3}{2}\big[d_d\langle i_{l1d}\rangle + d_q\langle i_{l1q}\rangle\big] \tag{3.35}$$

Equations (3.31)-(3.34) is divided into direct and quadrature component according to the equation (3.30)

$$\frac{d\langle i_{l1d}\rangle}{dt} = \frac{1}{L_1}\big[d_d\langle u_{in}\rangle - (r_{eq}+R_d)\langle i_{l1d}\rangle + R_d\langle i_{l2d}\rangle + w_sL_1\langle i_{l1q}\rangle - \langle u_{C_fd}\rangle\big] \tag{3.36}$$

$$\frac{d\langle i_{l1q}\rangle}{dt} = \frac{1}{L_1}\big[d_q\langle u_{in}\rangle - (r_{eq}+R_d)\langle i_{l1q}\rangle + R_d\langle i_{l2q}\rangle - w_sL_1\langle i_{l1d}\rangle - \langle u_{C_fq}\rangle\big] \tag{3.37}$$

$$\frac{d\langle i_{l2d}\rangle}{dt} = \frac{1}{L_2}\big[-(r_{l2}+R_d)\langle i_{l2d}\rangle + R_d\langle i_{l1d}\rangle + w_sL_2\langle i_{l2q}\rangle + \langle u_{C_fd}\rangle - \langle u_{od}\rangle\big] \tag{3.38}$$

$$\frac{d\langle i_{l2q}\rangle}{dt} = \frac{1}{L_2}\big[-(r_{l2}+R_d)\langle i_{l2q}\rangle + R_d\langle i_{l1q}\rangle - w_sL_2\langle i_{l2d}\rangle + \langle u_{C_fq}\rangle - \langle u_{oq}\rangle\big] \tag{3.39}$$

$$\frac{d\langle u_{C_fd}\rangle}{dt} = \frac{1}{C_f}\big[\langle i_{l1d}\rangle - \langle i_{l2d}\rangle + w_sC_f\langle u_{C_fq}\rangle\big] \tag{3.40}$$

$$\frac{d\langle u_{C_fq}\rangle}{dt} = \frac{1}{C_f}\big[\langle i_{l1q}\rangle - \langle i_{l2q}\rangle - w_sC_f\langle u_{C_fd}\rangle\big] \tag{3.41}$$

$$\langle i_{od}\rangle = \langle i_{\mathrm{l2d}}\rangle \tag{3.42}$$

$$\langle i_{oq}\rangle = \langle i_{l2q}\rangle \tag{3.43}$$

3.3 Steady-state operating point

The derived average model equations are used to solve the steady-state operating point. In order to solve operating points, the derivatives of the averaged valued model are set to zero and replaced their corresponding terms by upper case symbols.

Subsequent equations are represented in (3.44)-(3.53).

$$0 = D_d U_{in} - (r_{eq} + R_d) I_{l1d} + R_d I_{l2d} + w_s L_1 I_{l1q} - U_{C_f d} \tag{3.44}$$

$$0 = D_q U_{in} - (r_{eq} + R_d) I_{l1q} + R_d I_{l2q} - w_s L_1 I_{l1d} - U_{C_f q} \tag{3.45}$$

$$0 = -(r_{l2} + R_d) I_{l2d} + R_d I_{l1d} + w_s L_2 I_{l2q} + U_{C_f d} - U_{od} \tag{3.46}$$

$$0 = -(r_{l2} + R_d) I_{l2q} + R_d I_{l1q} - w_s L_2 I_{l2d} + U_{C_f q} - U_{oq} \tag{3.47}$$

$$0 = I_{l1d} - I_{l2d} + w_s C_f U_{C_f q} \tag{3.48}$$

$$0 = I_{l1q} - I_{l2q} - w_s C_f U_{C_f d} \tag{3.49}$$

$$I_{in} = \frac{3}{2}\Big[D_d I_{l1d} + D_q I_{l1q}\Big] \tag{3.50}$$

$$I_{od} = I_{l2d} \tag{3.51}$$

$$I_{oq} = I_{l2q} \tag{3.52}$$

In addition, a possible assumption is made for making the calculation simple. Current feedback is taken from the inverter side inductor to avoid complexities of using grid side inductor current as the resonance phenomena of LCL filter degrades the dynamics. It is better to take feedback current before filtering to get faster dynamics as well [38, 39]. Inverter safety is also ensured by this feedback arrangement. The aim of this thesis is to control reactive power at the point of common coupling. Thus, the inverter is not operated at the unity power factor. If the inverter is operated at the different power factor other than unity, then the assumption taken in [40] is invalid and the q component of inverter side inductor current cannot be neglected. It is assumed that U_{oq}=0 as the inductor currents are synchronized to the grid voltage. Furthermore, $U_{C_f d}$= U_{od} and $U_{C_f q}$= U_{oq} assumed and all resistive losses are neglected to solve the steady-state operating point easily. The operating points found in this procedure are almost close to the actual operating points. Equations (3.54)-(3.59) provide steady-state operating points symbolically. Numerical values of the steady-state operating point are listed in Table 3.3.

$$I_{l1d} = I_{l2d} \tag{3.53}$$

$$I_{l1q} = \frac{-D_d U_{in} + U_{od}}{w_s L_1} \tag{3.54}$$

$$I_{l1d} = \frac{2}{3}\frac{I_{in}}{D_d} - \frac{D_q}{D_d} I_{l1q} \tag{3.55}$$

Table 3.3 *Steady-state operating points*

I_{l1d}	Inductor current,d-component (Inverter-side)	$1.18 \times 10^3 A$
I_{l1q}	Inductor current,q-component (Inverter-side)	$59A$
I_{l2d}	Inductor current,d-component (Grid-side)	$1.18 \times 10^3 A$
I_{l2q}	Inductor current,q-component (Grid-side)	$6.18A$
D_d	Duty ratio,d-component	0.22
D_q	Duty ratio,q-component	0.104
U_{in}	Input voltage	$2500V$
U_{od}	Output voltage d-component	$563.38V$

$$I_{l2q} = I_{l1q} - w_s C_f U_{od} \tag{3.56}$$

$$D_d = \frac{U_{od} - w_s L_1 I_{l1q}}{U_{in}} \tag{3.57}$$

$$D_q = \frac{w_s L_1 I_{l1d}}{U_{in}} \tag{3.58}$$

Since the inverter is assumed to be operated at 1MW active and 50KVAr reactive power, I_{l1d} and I_{l1q} can be calculated from the power equation in the synchronous reference frame. active and reactive power in the synchronous reference frame.

$$\begin{aligned} P &= \frac{3}{2} U_{od} I_{l1d} = 10^6 W \\ I_{l1d} &= \frac{2}{3U_{od}} \times 10^6 \\ &= 1.18 \times 10^3 A \end{aligned} \tag{3.59}$$

$$\begin{aligned} Q &= \frac{3}{2} U_{od} I_{l1q} = 50 \times 10^3 VAr \\ I_{l1q} &= \frac{2}{3U_{od}} \times 50 \times 10^3 \\ &= 59A \end{aligned} \tag{3.60}$$

3.4 Linearized model

The non-linear averaged model found in the previous section. To obtain the state space representation of the non-linear average model, it is necessary to develop the linear model at the given operating points. The partial derivatives of all state, input and output variables are used to perform the linearization process. The derived

linear equations are given by

$$\frac{d\widehat{i}_{l1d}}{dt} = D_d\frac{\widehat{u}_{in}}{L_1} - \frac{r_{eq}+R_d}{L_1}\widehat{i}_{l1d} - \frac{1}{L_1}\widehat{u}_{Cfd} + \frac{R_d}{L_1}\widehat{i}_{l2d} + w_s\widehat{i}_{l1q} + \frac{U_{in}}{L_1}\widehat{d}_d \tag{3.61}$$

$$\frac{d\widehat{i}_{l1q}}{dt} = D_q\frac{\widehat{u}_{in}}{L_1} - \frac{r_{eq}+R_d}{L_1}\widehat{i}_{l1q} - \frac{1}{L_1}\widehat{u}_{Cfq} + \frac{R_d}{L_1}\widehat{i}_{l2q} - w_s\widehat{i}_{l1d} + \frac{U_{in}}{L_1}\widehat{d}_q \tag{3.62}$$

$$\frac{d\widehat{i}_{l2d}}{dt} = -\frac{r_{L2}+R_d}{L_2}\widehat{i}_{l2d} + \frac{1}{L_2}\widehat{u}_{Cfd} + \frac{R_d}{L_2}\widehat{i}_{l1d} + w_s\widehat{i}_{l2q} - \frac{1}{L_2}\widehat{u}_{od} \tag{3.63}$$

$$\frac{d\widehat{i}_{l2q}}{dt} = -\frac{r_{L2}+R_d}{L_2}\widehat{i}_{l2q} + \frac{1}{L_2}\widehat{u}_{Cfq} + \frac{R_d}{L_2}\widehat{i}_{l1q} - w_s\widehat{i}_{l2d} - \frac{1}{L_2}\widehat{u}_{oq} \tag{3.64}$$

$$\frac{d\widehat{u}_{Cfd}}{dt} = \frac{1}{C_f}\widehat{i}_{l1d} - \frac{1}{C_f}\widehat{i}_{l2d} + w_s\widehat{u}_{Cfq} \tag{3.65}$$

$$\frac{d\widehat{u}_{Cfq}}{dt} = \frac{1}{C_f}\widehat{i}_{l1q} - \frac{1}{C_f}\widehat{i}_{l2q} - w_s\widehat{u}_{Cfd} \tag{3.66}$$

$$\widehat{i}_{in} = \frac{3}{2}D_d\widehat{i}_{l1d} + \frac{3}{2}D_q\widehat{i}_{l1q} + \frac{3}{2}I_{l1d}\widehat{d}_d + \frac{3}{2}I_{l1q}\widehat{d}_q \tag{3.67}$$

$$\widehat{i}_{od} = \widehat{i}_{l2d} \tag{3.68}$$

$$\widehat{i}_{oq} = \widehat{i}_{l2q} \tag{3.69}$$

State space representation of linear equation (3.62)-(3.70) can be given in following from

$$\begin{aligned}\frac{d\widehat{\mathbf{x}}(t)}{dt} &= \mathbf{A}\widehat{\mathbf{x}}(t) + \mathbf{B}\widehat{\mathbf{u}}(t)\\ \widehat{\mathbf{y}}(t) &= \mathbf{C}\widehat{\mathbf{x}}(t) + \mathbf{D}\widehat{\mathbf{u}}(t)\end{aligned} \tag{3.70}$$

Where,
$\widehat{\mathbf{x}}(t)$=State variables=$\left[\widehat{i}_{l1d}, \widehat{i}_{l1q}, \widehat{i}_{l2d}, \widehat{i}_{l2q}, \widehat{u}_{Cfd}, \widehat{u}_{Cfq}\right]$
$\widehat{\mathbf{u}}(t)$=Input variables =$\left[\widehat{u}_{in}, \widehat{u}_{od}, \widehat{u}_{oq}, \widehat{d}_d, \widehat{d}_q\right]$
$\widehat{\mathbf{y}}(t)$=Output variables =$\left[\widehat{i}_{l1d}, \widehat{i}_{l1q}, \widehat{i}_{in}, \widehat{i}_{od}, \widehat{i}_{oq}\right]$

A, **B**, **C** and **D** are the state matrices. The equations (3.62) -(3.70) are used to obtain the elements of state matrices. **A**, **B**, **C** and **D** matrices with their associated

elements are given in equation (3.72) -(3.75)

$$\mathbf{A} = \begin{bmatrix} -\frac{(r_{eq}+R_d)}{L_1} & w_s & \frac{R_d}{L_1} & 0 & -\frac{1}{L_1} & 0 \\ -w_s & -\frac{(r_{eq}+R_d)}{L_1} & 0 & \frac{R_d}{L_1} & 0 & -\frac{1}{L_1} \\ \frac{R_d}{L_2} & 0 & -\frac{(r_{eq}+R_d)}{L_2} & w_s & -\frac{1}{L_1} & 0 \\ 0 & \frac{R_d}{L_2} & -w_s & -\frac{(r_{eq}+R_d)}{L_2} & 0 & -\frac{1}{L_1} \\ \frac{1}{C_f} & 0 & -\frac{1}{C_f} & 0 & 0 & w_s \\ 0 & \frac{1}{C_f} & 0 & -\frac{1}{C_f} & -w_s & 0 \end{bmatrix} \tag{3.71}$$

$$\mathbf{B} = \begin{bmatrix} \frac{D_d}{L_1} & 0 & 0 & \frac{U_{in}}{L_1} & 0 \\ \frac{D_q}{L_1} & 0 & 0 & 0 & \frac{U_{in}}{L_1} \\ 0 & -\frac{1}{L_2} & 0 & 0 & 0 \\ 0 & 0 & -\frac{1}{L_2} & 0 & 0 \\ 0 & 0 & 0 & 0 & 0 \\ 0 & 0 & 0 & 0 & 0 \end{bmatrix} \tag{3.72}$$

$$\mathbf{C} = \begin{bmatrix} 1 & 0 & 0 & 0 & 0 & 0 & 0 \\ 0 & 1 & 0 & 0 & 0 & 0 & 0 \\ \frac{3}{2}D_d & \frac{3}{2}D_q & 0 & 0 & 0 & 0 & 0 \\ 0 & 0 & 1 & 0 & 0 & 0 & 0 \\ 0 & 0 & 1 & 0 & 0 & 0 & 0 \end{bmatrix} \tag{3.73}$$

$$\mathbf{D} = \begin{bmatrix} 0 & 0 & 0 & 0 & 0 \\ 0 & 0 & 0 & 0 & 0 \\ 0 & 0 & 0 & \frac{3}{2}I_{l1d} & \frac{3}{2}I_{l1q} \\ 0 & 0 & 0 & 0 & 0 \\ 0 & 0 & 0 & 0 & 0 \end{bmatrix} \tag{3.74}$$

Transfer function of input and output variables can be found by taking laplace transform of equation (3.71) and converted to the equation represented in equation (3.77)

$$\begin{aligned} s\mathbf{X}(s) &= \mathbf{A}\mathbf{X}(s) + \mathbf{B}\mathbf{U}(s) \\ \mathbf{Y}(s) &= \mathbf{C}\mathbf{X}(s) + \mathbf{D}\mathbf{U}(s) \end{aligned} \tag{3.75}$$

$$\begin{aligned}\mathbf{Y}(s) &= \big[\mathbf{C}\big((s)\mathbf{I}-\mathbf{A}\big)\big)^{-1}\mathbf{B}+\mathbf{D}\big]\mathbf{U}(s)\\ &= \mathbf{G}\mathbf{U}(s)\end{aligned} \tag{3.76}$$

Where, **G** is the transfer function matrix and its associated matrix elements are given in equation (3.78).

$$\begin{bmatrix}\widehat{i}_{l1d}\\ \widehat{i}_{l1q}\\ \widehat{i}_{in}\\ \widehat{i}_{od}\\ \widehat{i}_{oq}\end{bmatrix} = \begin{bmatrix}G_{ild-o} & T_{old-o} & T_{olqd-o} & G_{cld-o} & G_{clqd-o}\\ G_{ilq-o} & T_{oldq-o} & T_{olq-o} & G_{cldq-o} & G_{clq-o}\\ Y_{in} & T_{oid-o} & T_{oiq-o} & G_{cid-o} & G_{ciq-o}\\ G_{iod-o} & -Y_{od-o} & -Y_{oqd-o} & G_{cod-o} & G_{coqd-o}\\ G_{ioq-o} & -Y_{odq-o} & -Y_{oq-o} & G_{codq-o} & G_{coq-o}\end{bmatrix}\begin{bmatrix}\widehat{u}_{in}\\ \widehat{u}_{od}\\ \widehat{u}_{oq}\\ \widehat{d}_{d}\\ \widehat{d}_{q}\end{bmatrix} \tag{3.77}$$

According to previous study active and reactive power control is done by controlling $\widehat{i}_{l1d}$ and $\widehat{i}_{l1q}$ respectively. To establish stable control in $\widehat{i}_{l1d}$ and in $\widehat{i}_{l1q}$, frequency response of G_{cld-o} and G_{clq-o} is analyzed in the subsequent chapter.

4. CONTROL TECHNIQUES USED FOR CONTROLLING REACTIVE POWER

This chapter presents step by step followed control techniques to control reactive power. In inner current control, the PI controller is used to control the output converter current. Besides, an outer controller is designed to generate the current reference for the previously designed PI controller. As a result, control of active and reactive power is possible. The detailed process of active power control is not shown here. It is beyond the scope of this thesis. Furthermore, the grid synchronization process is involved from the beginning of the GCC model design for making sure that converter is properly connected with the grid.

4.1 Control block diagram implementation

To keep grid voltage and frequency in an acceptable limit, the grid supporting power converter regulates its active and reactive power accordingly [13]. Different control strategies have been proposed as described in the earlier chapter. Droop control is an attractive solution for its simplicity, low cost, and easy implementation [22]. In this thesis, droop control mechanism is applied to regulate active and reactive power in order to support the grid. The current references of inner current controllers are generated from the droop mechanism. Q-V droop is used generate a current reference for reactive power control whereas P-f droop is used to generate a current reference for real power control. The block diagram which is used to regulate active and reactive power is given in Figure 4.1 [13]. In this figure, the PI controller is used to control the d and q component of converter output current, those are generated from Clarke's transformation based on the synchronous reference frame. Grid angle θ is estimated using SRF-PLL.

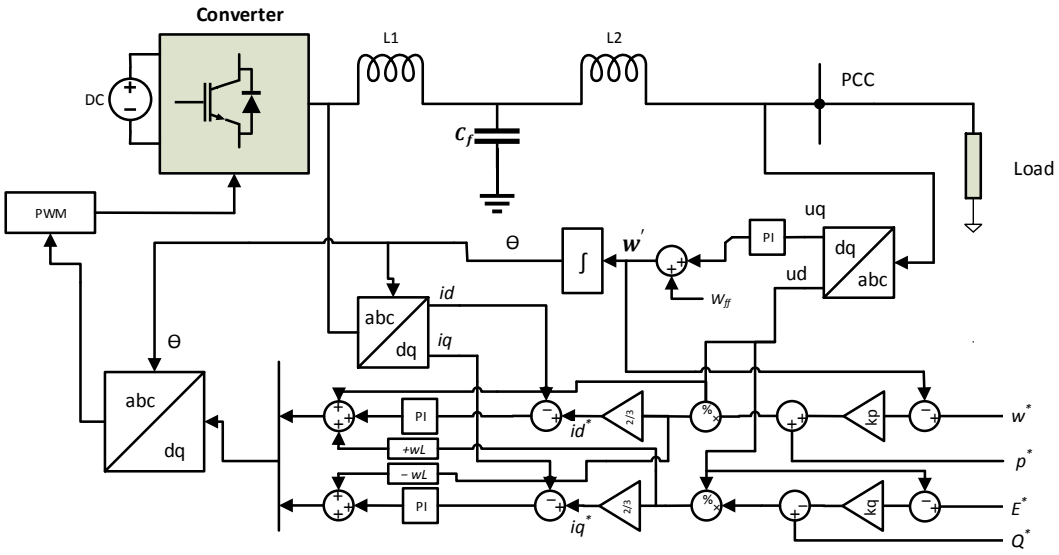

Figure 4.1 *Block diagram of power control in GCC*

4.2 Grid synchronization

When the converter is connected to the grid, it is required to determine grid frequency and angle to synchronize its AC side currents with grid voltage. This information is also needed for the operation of its control loop. Various synchronization techniques are used to perform grid synchronization in the grid-connected converter. Among them, SRF-PLL is simple and its implementation is easy. In this thesis, SRF-PLL is chosen to synchronize GCC to the grid. However, SRF-PLL does not possess satisfactory performance during the unbalanced grid condition [41]. Considering this matter, the balanced grid condition is assumed.

4.2.1 Control design of SRF-PLL

The SRF-PLL control block is formed with a transformation block, the PI controller and an integrator. The transformation block is used to convert sensed three-phase sinusoidal signals of the grid into two dc valued signal U_q and U_d. One of the two DC valued signals is taken to compare with the reference value. In this design, U_q is used to compare with the reference q component voltage. Conventionally, the reference of the q component voltage is zero. An error value is produced from that

comparison which is then sent to the PI controller. Elimination of steady-state error value is done by the PI controller. The controller output is added to the grid nominal frequency. Later, the added frequency is converted to a phase angle by an integrator, and it is then feedback to the transformation block resulting in a closed loop control.

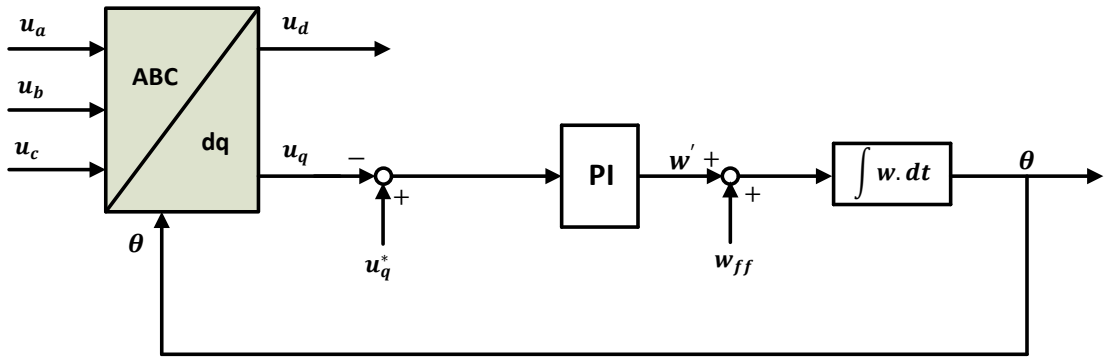

Figure 4.2 *Control block diagram of SRF-PLL*

To establish a stable and efficient control, it is needed to analyze the small signal model of SRF-PLL. Small signal modeling is presented in [24, 42]. Linearized control block diagram resulting from small signal modeling is given in Figure 4.2. It is not discussed further in this thesis. Taking the plant transfer function G_p from [24, 42] and closed loop gain with the controller is calculated in equation (4.2), where G_c is the controller transfer function.

$$G_p = \frac{U_{od}}{s} \tag{4.1}$$

$$L_{pll} = G_p G_c \tag{4.2}$$

PI controller transfer function is organized in the following equation

$$G_c = \frac{-1K_k(\frac{s}{w_z} + 1)}{s} \tag{4.3}$$

In order to reach steady-state condition quickly, fast control dynamics is needed. Thus, high control bandwidth is required. However, the negative resistor like the behavior of the impedance, causing instability at lower frequency makes the use of control bandwidth limited. Generally, the low crossover frequency is used in SRF-PLL to avoid instability due to impedance based interaction in the grid-connected converter [43].

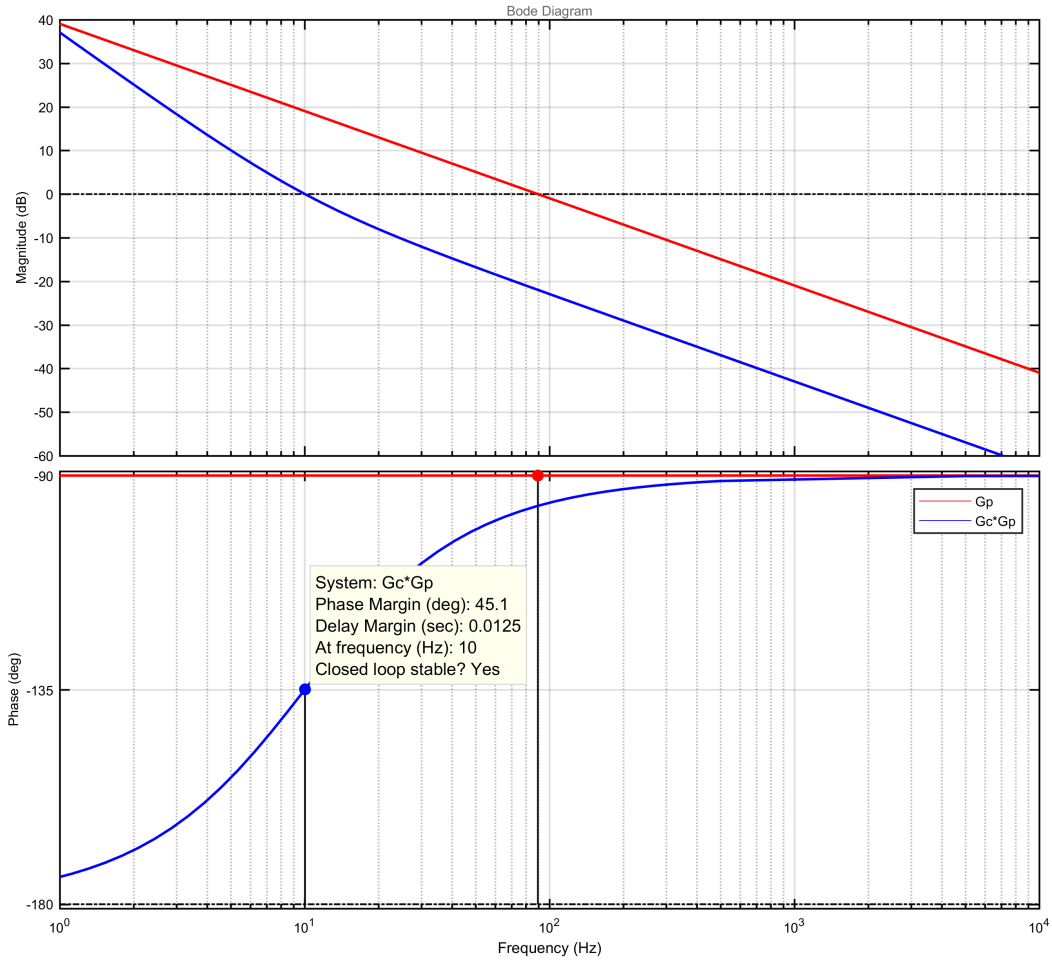

Figure 4.3 *SRF-PLL loop gain frequency response*

Controller tuning is done by using the loop shaping technique. According to loop shaping technique, a zero is placed at ten hertz to boost phase and gain K_k is selected to get 10 Hz crossover frequency and the phase margin of 45°. Plant loop gain and closed loop gain with the controller is demonstrated in Figure 4.3.

4.3 Inner current control

Figure 4.4, illustrates a generalized block diagram of output current control of an inverter where the output current is taken from the grid side inductor and converted to dq domain. The transformed d and q component of inverter output current are then controlled using negative feedback and PI controllers. The outputs of the PI

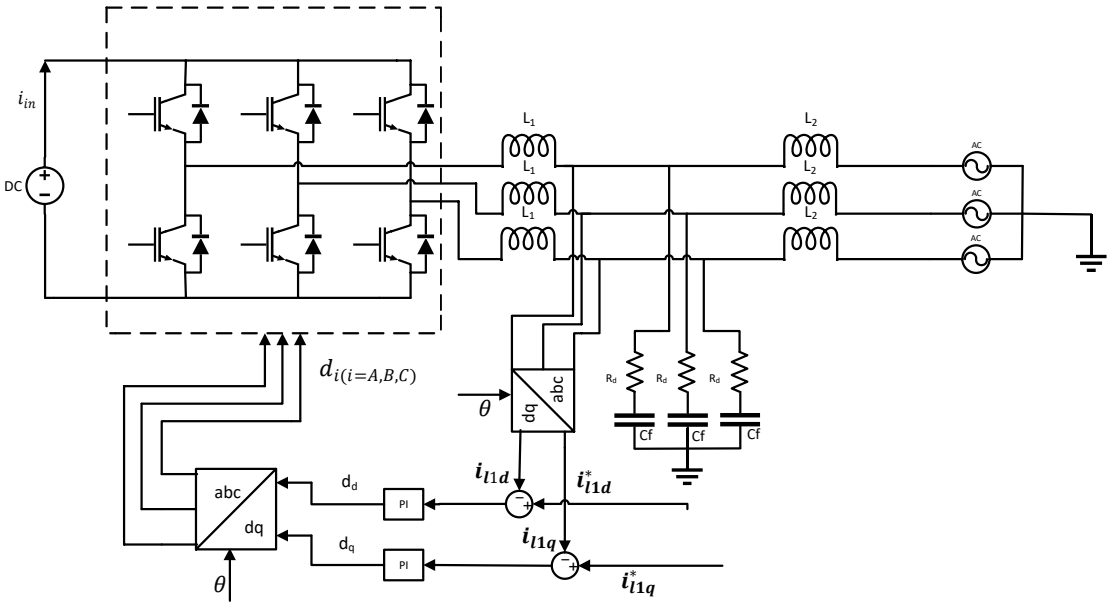

Figure 4.4 *Output current control in dq domain*

controllers are duty cycles in dq domain. The duty cycles are generated from the controllers according to the following simple control equation.

$$d_d = G_{PI}(i^*_{l1d} - i_{l1d}) \tag{4.4}$$

$$d_q = G_{PI}(i^*_{l1q} - i_{l1q}) \tag{4.5}$$

The transfer functions found in Chapter 3, allows representing input-output dynamics in the equation given in (4.6)-(4.8). The output current is taken from the converter side inductor of the LCL filter connected in between grid and the converter. For the simplicity, cross-coupling terms are neglected in input-output dynamics.

$$\widehat{i}_{l1d} = G_{ild-o}\widehat{u}_{in} + T_{old-o}\widehat{u}_{od} + T_{olqd-o}\widehat{u}_{oq} + G_{cld-o}\widehat{d}_d + G_{clqd-o}\widehat{d}_q \tag{4.6}$$

$$\widehat{i}_{l1q} = G_{ilq-o}\widehat{u}_{in} + T_{oldq-o}\widehat{u}_{od} + T_{olq-o}\widehat{u}_{oq} + G_{cldq-o}\widehat{d}_d + G_{clq-o}\widehat{d}_q \tag{4.7}$$

$$\widehat{i}_{in} = Y_{in}\widehat{u}_{in} + T_{oid-o}\widehat{u}_{od} + T_{oiq-o}\widehat{u}_{oq} + G_{cid-o}\widehat{d}_d + G_{ciq-o}\widehat{d}_q \tag{4.8}$$

Figure 4.5 and 4.6 are the reduced order output dynamics neglecting cross-coupling terms. Where G_{PI} and H are the controller transfer function and sensing gain respectively. G_{SPWM} is the modulator gain. Moreover, those figures illustrate the

current control loop gain in d and q channel, given in (4.9)-(4.10).

$$L_{out_d} = G_{cld-o} G_{SPWM} G_{PI-d} H_d \tag{4.9}$$

$$L_{out_q} = G_{clq-o} G_{SPWM} G_{PI-q} H_q \tag{4.10}$$

According to (4.8), control engineering block diagram of input dynamics is rep-

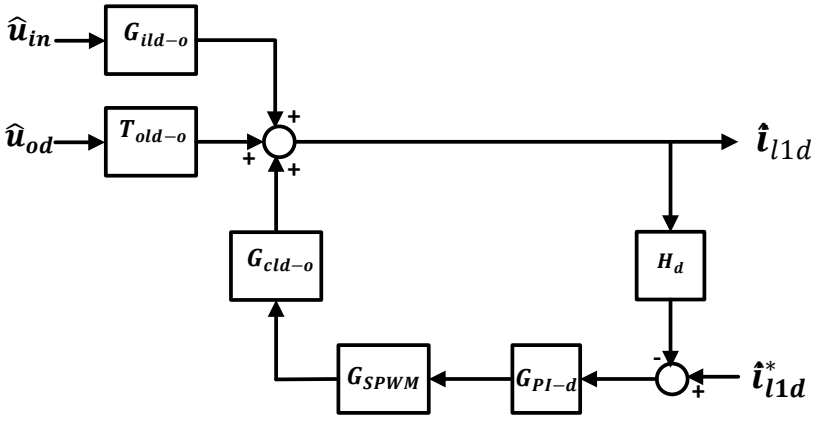

Figure 4.5 *Reduced order output dynamics of d-channel*

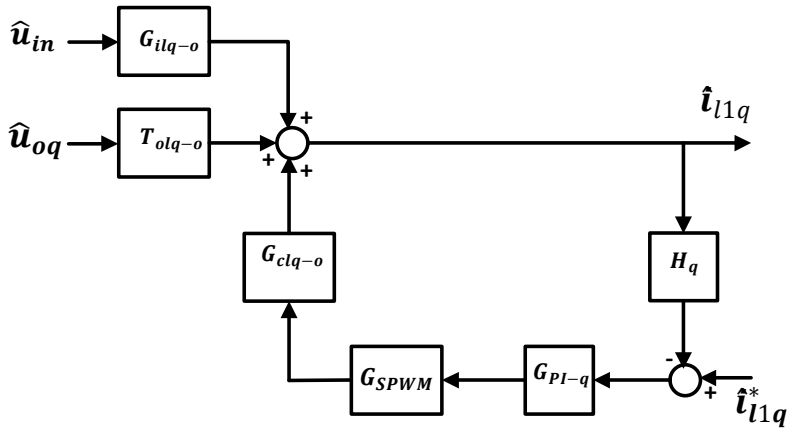

Figure 4.6 *Reduced order output dynamics of q-channel*

resented in Figure 4.7 and 4.8. Since, the aim of this thesis is not operate the converter in the unity power factor for sharing reactive power to the grid, input dynamics depends on both d and q component.

The controller parameters are selected in such a way that control dynamics G_{cld-o} and G_{clq-o} in open loop shows stable characteristics at the closed loop. Therefore,

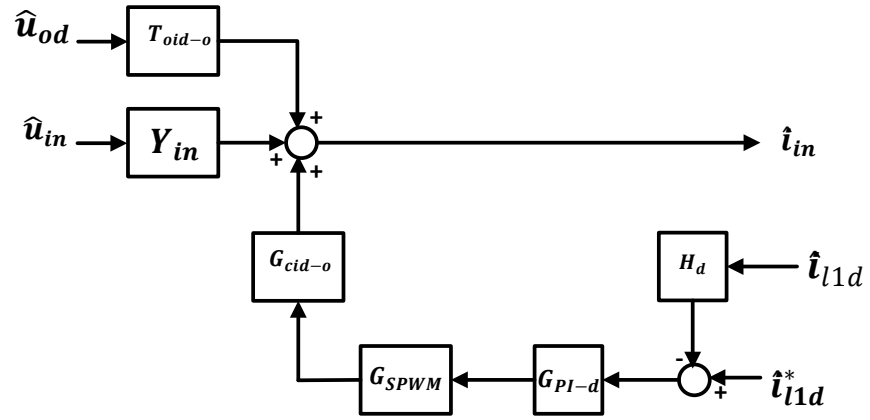

Figure 4.7 *Reduced order input dynamics of d-channel*

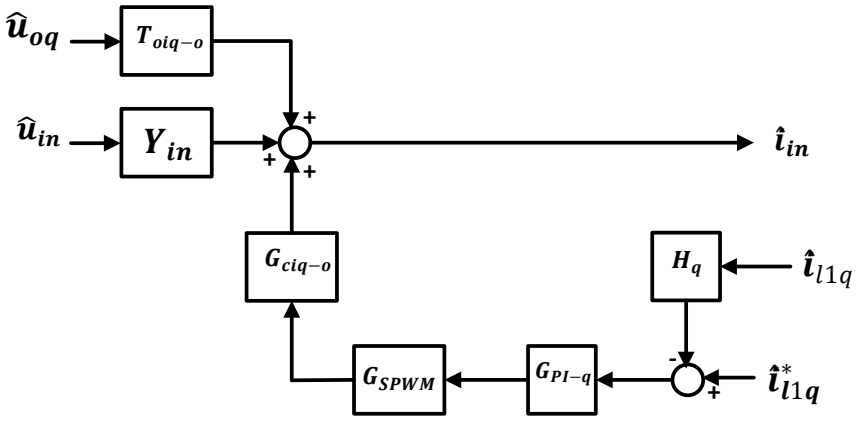

Figure 4.8 *Reduced order input dynamics of q-channel*

G_{cld-o} at the open loop is plotted in the figure. Since, d and q channel output dynamics are the same only d channel frequency response is plotted in Figure 4.9. Figure 4.9, depicts that, the phase of the open loop output dynamics starts from the zero degrees. It indicates that a negative feedback controller is needed to stabilize converter output. Moreover, the resonance appears in the frequency response due to the deployment of the LCL filter. Keeping this in mind, it is hard to implement the faster controller. In such a case, the crossover frequency below the maximum possible crossover frequency is chosen. It is mentioned in [44] that, maximum loop crossover frequency is $\frac{f_{sw}}{5}$. A simple PI controller with the crossover frequency of 300Hz is used. Later, proper poles and zeroes are placed according to controller

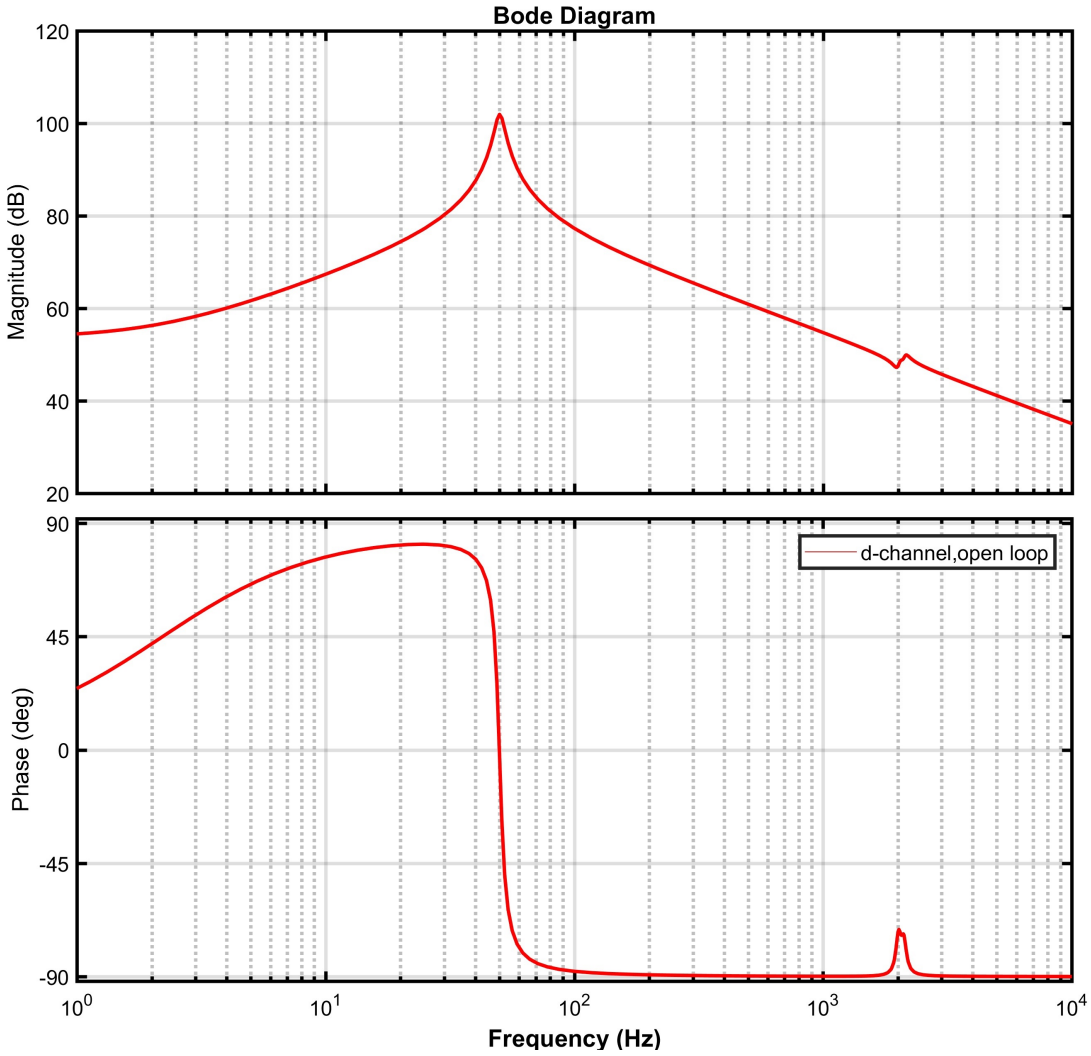

Figure 4.9 *Open loop d-channel frequency response*

transfer function given in (4.11) for stable control operation.

$$G_{PI-d} = G_{PI-q} = \frac{K_c(\frac{s}{w_z} + 1)}{s} \tag{4.11}$$

In the controller transfer function, an LHP zero at the 215Hz frequency is selected to boost the phase around the crossover frequency. It gives the phase margin of around 55. Controller gain is selected, so that crossover frequency is precisely 300Hz. Controller transfer functions with its associated parameters are given in (4.12).

$$G_{PI-d} = G_{PI-q} = \frac{10^{-4.66/20}(\frac{s}{2*pi*215} + 1)}{s} \tag{4.12}$$

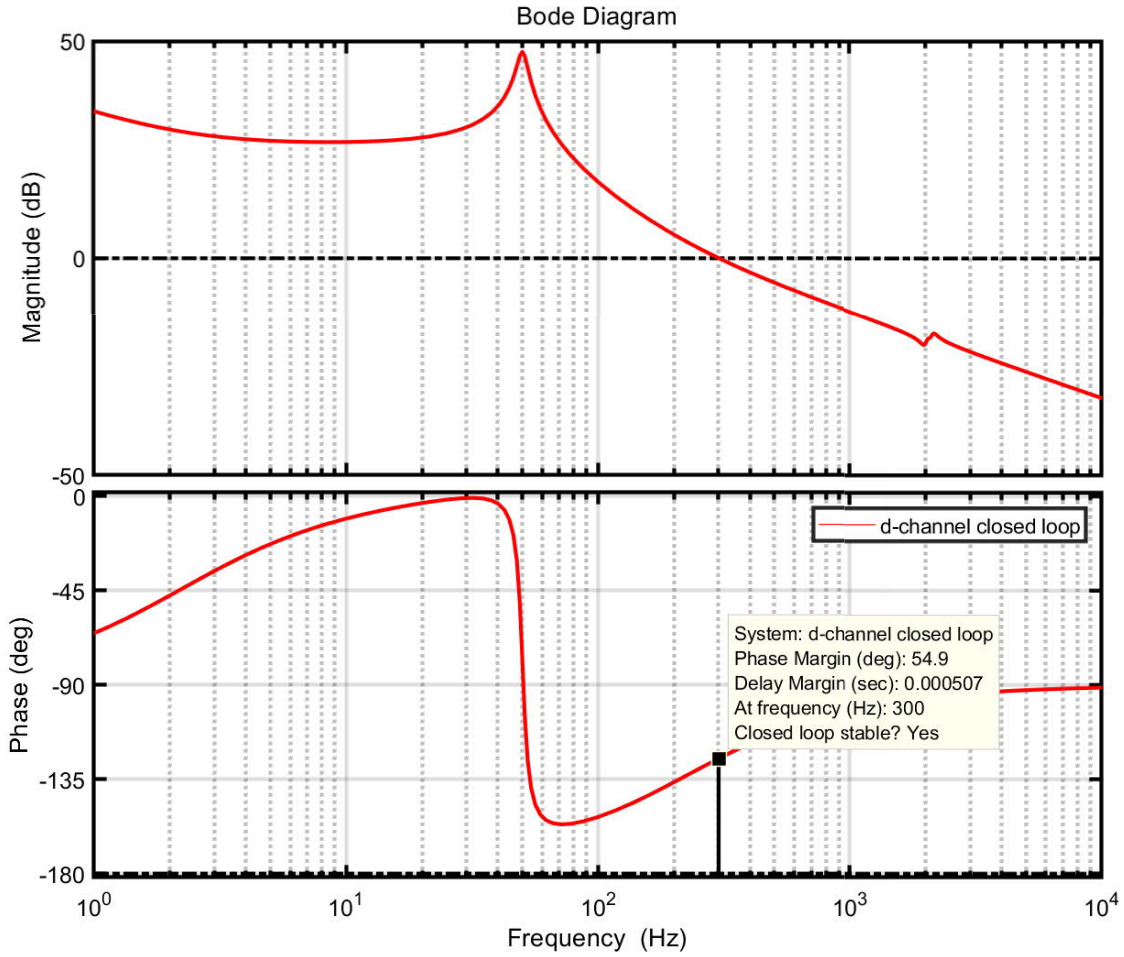

Figure 4.10 *Closed loop d-channel frequency response*

Figure 4.10, illustrates the closed loop frequency response after controller implementation. This figure shows that a closed loop is stable with a phase margin of 55 and a crossover frequency of 300Hz. As, d and q channel transfer function is identically the same, both of the channel exhibit the same frequency response. Thus control parameters setting is precisely the same in each case. Only, the d channel frequency response is documented.

4.3.1 Decoupling gains

The cross-coupling terms which were neglected in the previous analysis for inner current control now have to be taken in to account. It is needed in order to nullify the coupling effect in the dynamics of d and q components in current control. Coupling effect may degrade the control performance in the transient period [24]. Decoupling gains can be calculated from the linearized output dynamics of d and q component discussed in the previous chapter.

$$\frac{d\widehat{i}_{l1d}}{dt} = \frac{1}{L_1}(-r_{eq}\widehat{i}_{l1d} + w_s L_1 \widehat{i}_{l1d} + D_d\widehat{u}_{in} - \widehat{u}_{od} + U_{in}\widehat{d}_d) \tag{4.13}$$

Adding a new value with the $\widehat{d}_d$ which provides the above equation without the coupling terms and the equating would be the solution of getting decoupling gain.

$$\frac{1}{L_1}(-r_{eq}\widehat{i}_{l1d}+D_d\widehat{u}_{in}-\widehat{u}_{od}+U_{in}\widehat{d}_d) = \frac{1}{L_1}(-r_{eq}\widehat{i}_{l1d}+w_s L_1\widehat{i}_{l1q}+D_d\widehat{u}_{in}-\widehat{u}_{od}+U_{in}(\widehat{d}_d+\widehat{d}_{dx}) \tag{4.14}$$

$$\widehat{d}_{dx} = -\frac{w_s L_1}{U_{in}}\widehat{i}_{l1q} \tag{4.15}$$

Similarly for the q channel, decoupling gain is,

$$\widehat{d}_{qx} = \frac{w_s L_1}{U_{in}}\widehat{i}_{l1d} \tag{4.16}$$

The current control block diagram generated after applying decoupling gain is given in Figure 4.11. After the process of current control and applied decoupling gains to reduce the cross-coupling effect, Figure 4.12, shows that d and q component current is stable in the steady-state. In addition to that, it is observed that there is no cross-coupling effect present in the step response of the q component current.

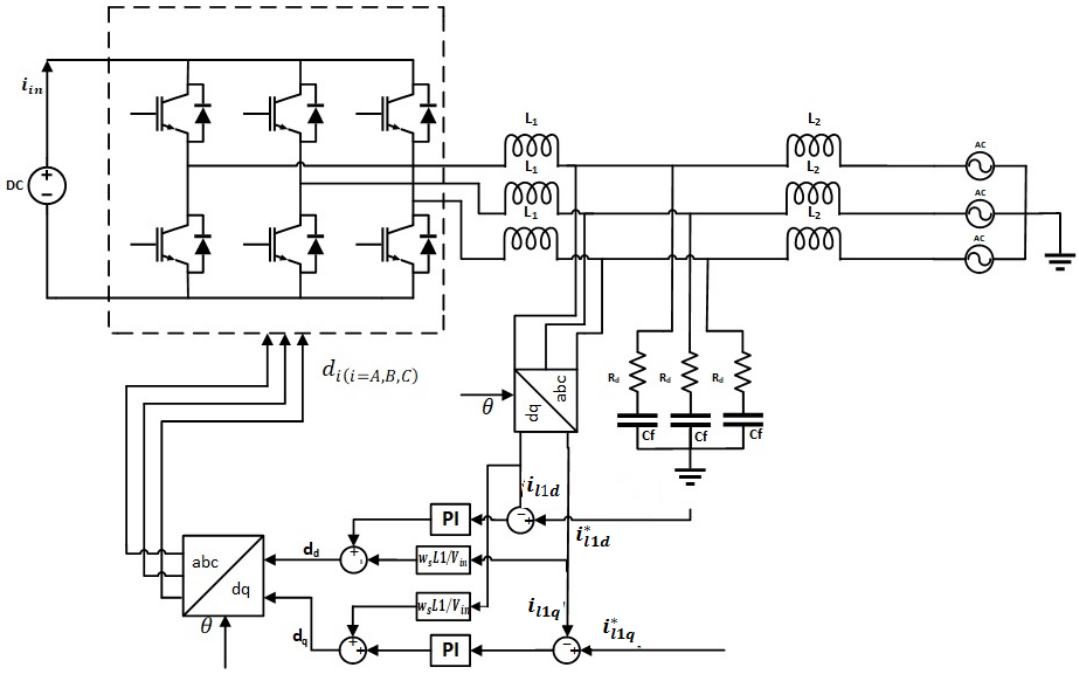

Figure 4.11 *Current control when decoupling gain is applied*

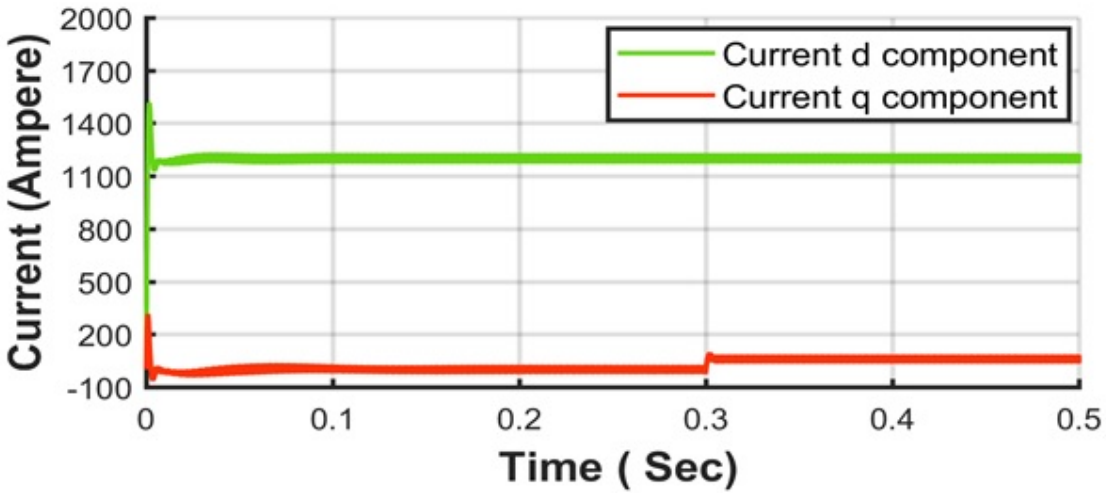

Figure 4.12 *Step response of current when decoupling gain is applied*

4.4 Reactive power control

Active and reactive power control depends on the generation of current reference according to the control requirement. Conventionally, reactive power is controlled by changing the reference of q component current whereas active power is controlled

by changing the reference of the d component. To control reactive power, q component current reference is changed according to the Q-V droop equation (2.30). However droop equation is modified to obtain droop controller gain according to the block diagram presented in Figure 4.1 from Chapter 4. Similarly, active power is controlled by changing d component current reference according to droop method. However, variation is observed with different line impedances connected to the converter. Reference current calculation and droop equation is given below for easy understanding.

$$i_{l1q}^{*} = \frac{2}{3}\frac{Q}{u_d} \tag{4.17}$$

$$E^{*} - E = n(Q^{*} - Q) \tag{4.18}$$

According to the block diagram presented in Figure 4.1 in Section 4.1, droop equation is rearranged in (4.19)-(4.22). Figure 4.13 has been drawn according to (4.22).

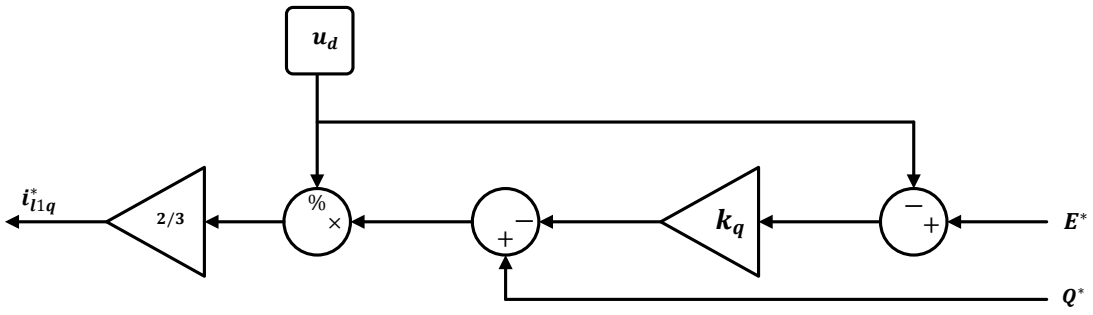

Figure 4.13 *Reference generation for reactive power control*

$$\frac{(E^{*} - u_d)}{n} = Q^{*} - Q \tag{4.19}$$

$$(E^{*} - u_d)k_q = Q^{*} - Q \quad where, \quad k_q = \frac{1}{n} \tag{4.20}$$

$$Q = Q^{*} - (E^{*} - u_d)k_q \tag{4.21}$$

Where,

u_d= Grid voltage d-component

k_q=Droop controller gain

Q^{*}=Reference reactive power

Q= Calculated reactive power to generate reactive current reference

Droop co-efficient selection: Q-V droop coefficient is calculated according to [45, 46, 21] . It is given in the equation

$$n = \frac{\Delta U_{normal}}{\Delta Q_{max}} \tag{4.22}$$

ΔU_{normal}= is the maximum acceptable voltage deviation at the PCC according to IEEE standard.
ΔQ_{max} depends on the operating power factor of the converter. Droop co-efficient is decreased when reactive power capacity of the converter increased.
In this thesis, the converter is assumed to operate at 0.99 power factor initially. It is calculated that, at 0.99 power factor, the designed converter can supply or absorb 50KVAr reactive power. Therefore, the maximum reactive power deviation capacity of the converter is 100KVAr.

$$n = \frac{\Delta U_{normal}}{\Delta Q_{max}} = \frac{(563 \times 1.05) - (563 \times 0.95)}{100 \times 10^3} = 0.000563 \tag{4.23}$$

Controller gain is calculated in the following.

$$k_q = \frac{1}{n} = \frac{1}{0.000563} = 1776 \tag{4.24}$$

5. DESIGN VERIFICATION AND DISCUSSION

The chapter presents the performance of the designed converter model. Performance is investigated by connecting the developed model to the high voltage, medium voltage, and low voltage transmission line. Test results while connecting to the transmission line of different voltage levels are presented and analyzed in this chapter. The model used to evaluate the performance of a droop controlled grid-connected converter is given in Figure 5.1. In this simulation model coupling transformer is used to connect converter with the high and medium voltage transmission line. The converter is connected directly to the low voltage transmission line as the voltage levels are the same in both converter and low voltage transmission line. Step changing mechanism is used to observe the performance of reactive power control (droop control) during the change of grid voltages.

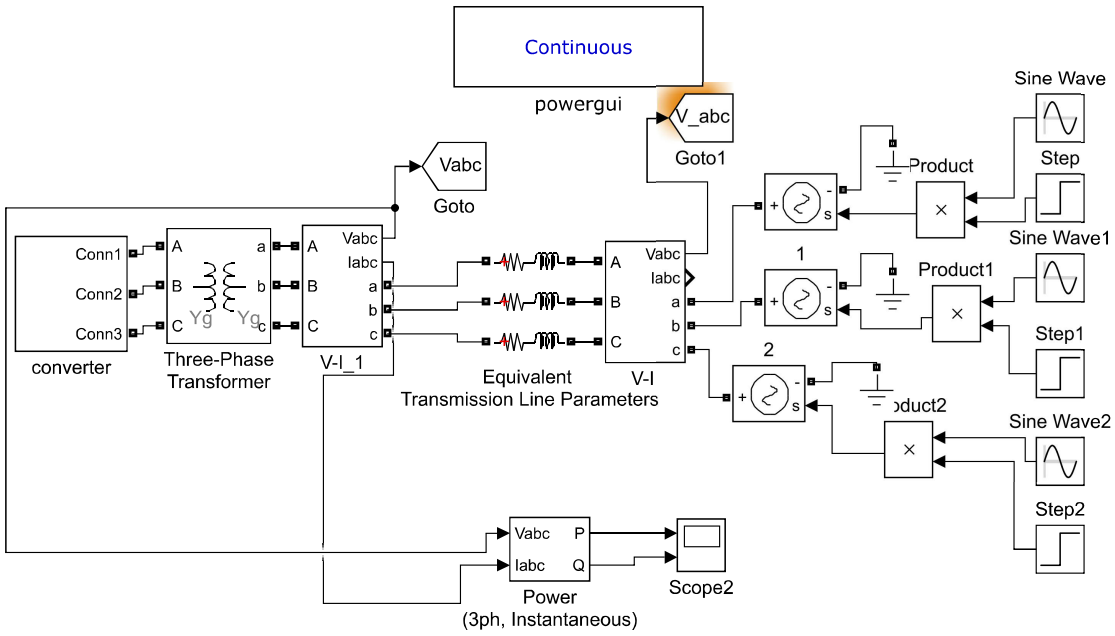

Figure 5.1 *Simulation model to evaluate performance of droop controlled converter*

5.1 Test case 1: Droop control verification in high voltage line.

Droop performance is analyzed in the high voltage grid. The converter model is connected to the high voltage ac source through a step up coupling transformer and a 200 km high voltage transmission line. High voltage transmission line is composed of proper resistive and inductive parameters. In this case, resistance of 0.06 ohm/km and reactance of 0.191 ohm/km is used to design 200 km transmission line

5.1.1 Case A: Increased grid voltage

The step change of 5% increased grid voltage is applied to observe the reactive power condition and its associated q component of current. The step change is applied at the 0.3 s of simulation time.

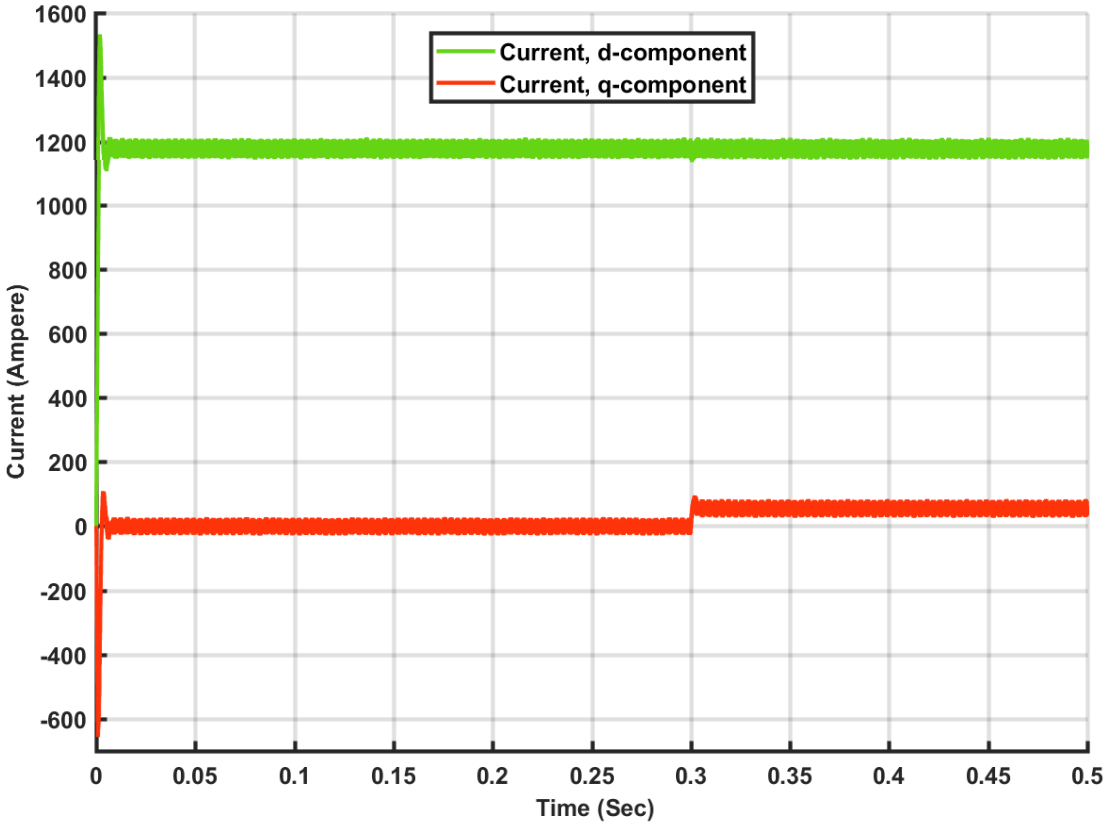

Figure 5.2 *Current condition when step change of increased grid voltage applied.*

Figure 5.2, below is a simulation time Vs dq component of current curve. Current component, d is taken from the input of an inner current controller whereas q component is taken from q component of inner current controller. Since, reference of d component of current controller is unchanged during the simulation time, d component of current remains same after the step change in grid voltage.From the graph it is clear that q component current is significantly increased after the step change is applied. according to the power theory in synchronous reference frame, the increased reactive component of current allows the converter model to absorb reactive power from the grid. The power curve from Figure 5.3, also indicates that reactive power is negative after the step change in grid voltage, which basically means the converter is absorbing reactive power from the grid. Moreover, the power curve indicates that active power is also increased from the rated value at the point of step change because active power control is not implemented here. On the other hand, the current component of active power is controlled. Active power could be controlled by using P-f droop implementation to change the reference value of d component current in inner current control.

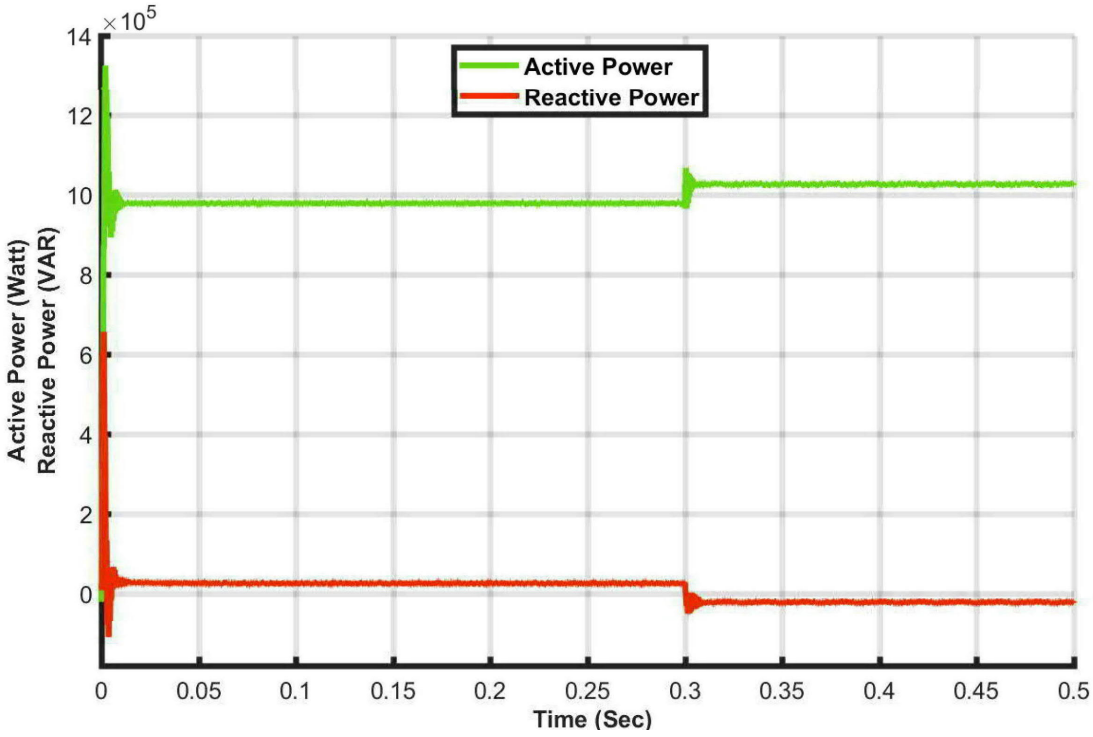

Figure 5.3 *Power condition when step change of increased grid voltage applied*

5.1.2 Case B: Decreased grid voltage

Reactive power control is verified by bidirectional control performance. In this case, it is demonstrated, control is working when the voltage at the point of common coupling is decreased from the nominal value. The reduced voltage at the PCC allows the converter to activate its control. Reactive power supply from the converter control is expected to raise the voltage label at the PCC. A simple model like Figure 1 is used to verify this operation. The step change of 95% from the nominal grid value is applied at the 0.3 s of simulation time. Figure 5.4 shows the corresponding simulation result From the figure, it is observed that at 0.3sec of simulation time,

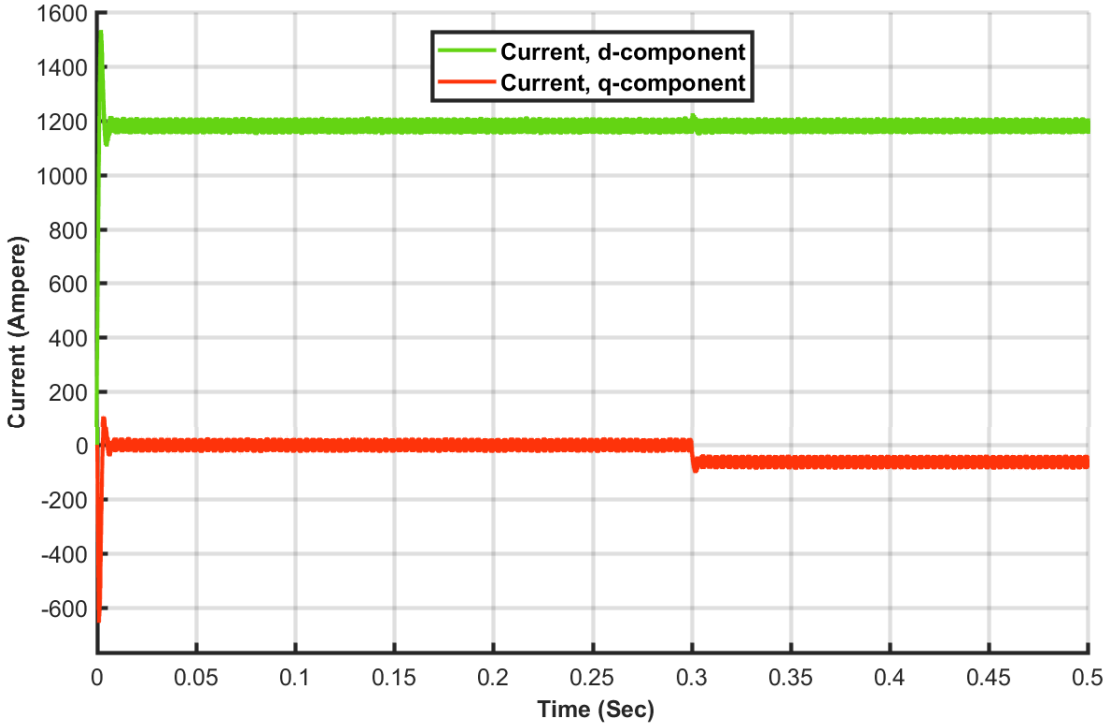

Figure 5.4 *Current condition when step change of decreased grid voltage applied.*

the coupling point voltage is reduced to 95% of nominal value. It happens in the grid when reactive power demand is higher than the production due to the immediate connections of an inductive load in the network or the network fault. Providing reactive power to the point of interconnection is the possible way of reducing the effect of reactive power imbalance. From Figure 5.4, it is clear that 0.3 sec of simulation time and after that q component current is negative. The negative amount of current which indicates that a certain amount of reactive power is supplying to the point of common coupling. Supplied reactive power is realized from Figure 5.5,

at 0.3 s of simulation time where the step change is applied. Reduced amount of active power is also appeared in the graph due to the effect of the decreased value of d component grid voltage.

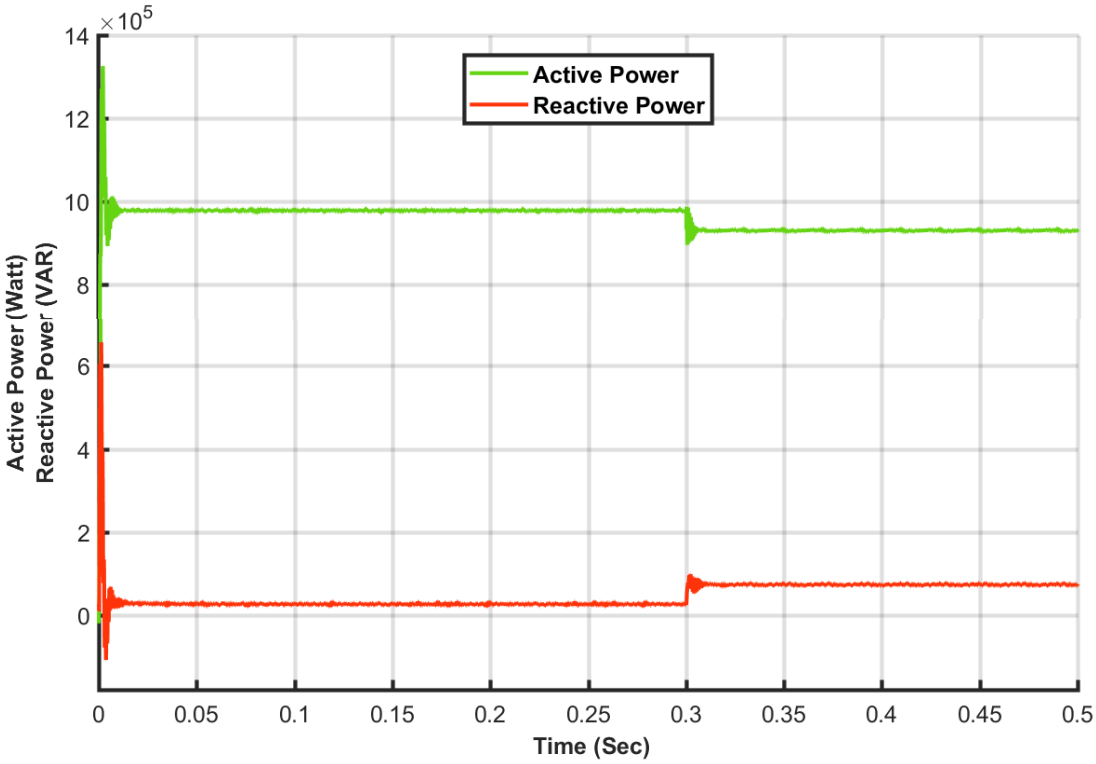

Figure 5.5 *Power condition when step change of decreased grid voltage applied.*

5.2 Test case 2: Droop control verification in medium voltage line.

The model is tested in 20 KV medium voltage transmission line. The transmission line is 150 km long. Transmission line parameters are 0.161 ohm/km, 0.191 resistance and inductance are used respectively. Observation of droop performance is then done by connecting the designed converter model to the grid, through a 690/20 KV step-up transformer. The process of applying step change in grid voltage is followed. Later, the simulation result is analyzed to verify droop performance in the Medium voltage transmission line. Furthermore, droop control stability is observed while changing the line resistance, corresponding $\frac{R}{X}$ ratio is listed in table 5.1 as well.

5.2.1 Case A: Increased grid voltage

Reactive power condition and its corresponding controlling component are observed here with the step change of 5% increased grid voltage from the nominal value. Grid voltage is increased due to the excessive amount of reactive power available in the network. To balance the amount of reactive power it needs to extract reactive power from the grid. Thus, this case reactive power is absorbed by the converter with the help of the q component current controller. Figure 5.6, shows the dq component of current at the duration of step change applied and before it is applied. It is observed that q component of current is likely to the high voltage test case. From Figure 5.7,

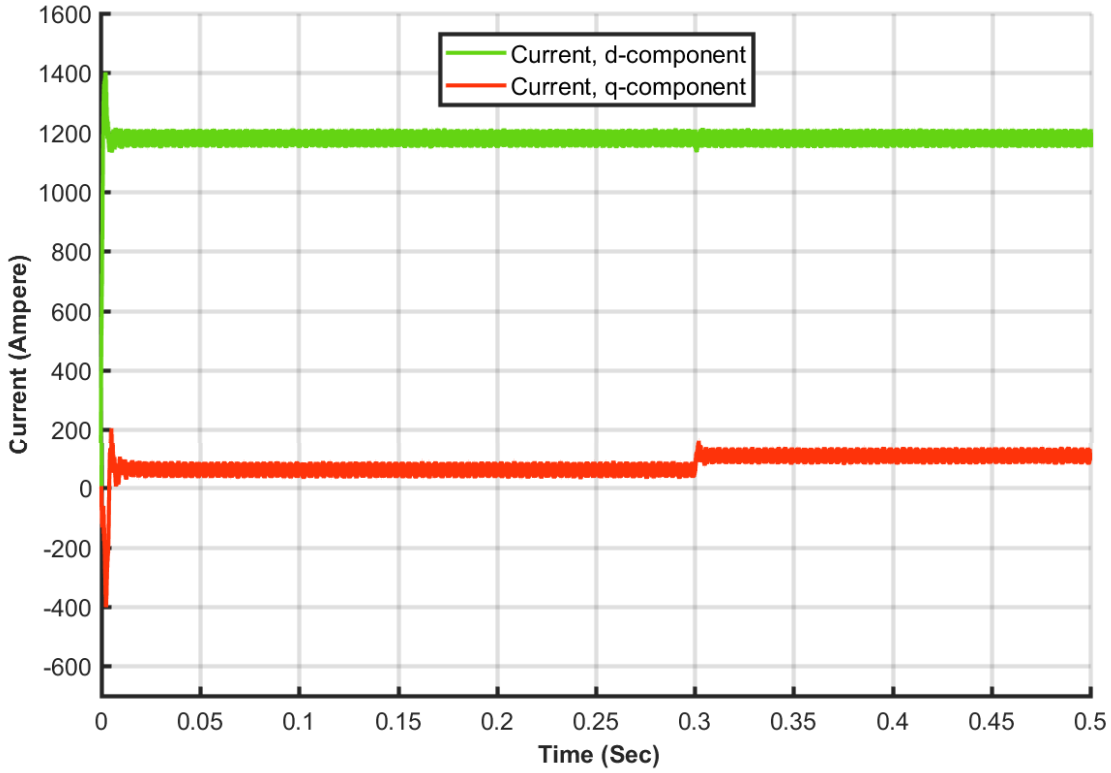

Figure 5.6 *Current condition when step change of increased grid voltage applied.*

it is clear that the power curve is similar to the case of the high voltage transmission line. In this case, a certain amount of reactive power is absorbing from the grid. Thus, it is concluded that droop control in the medium voltage transmission line is stable. However, it attains the unstable state when the line resistance is increased to a great amount. Great amount of resistance indicates also much high $\frac{R}{X}$. Figure 5.8, shows a comparison of stable and unstable condition of currents in a situation

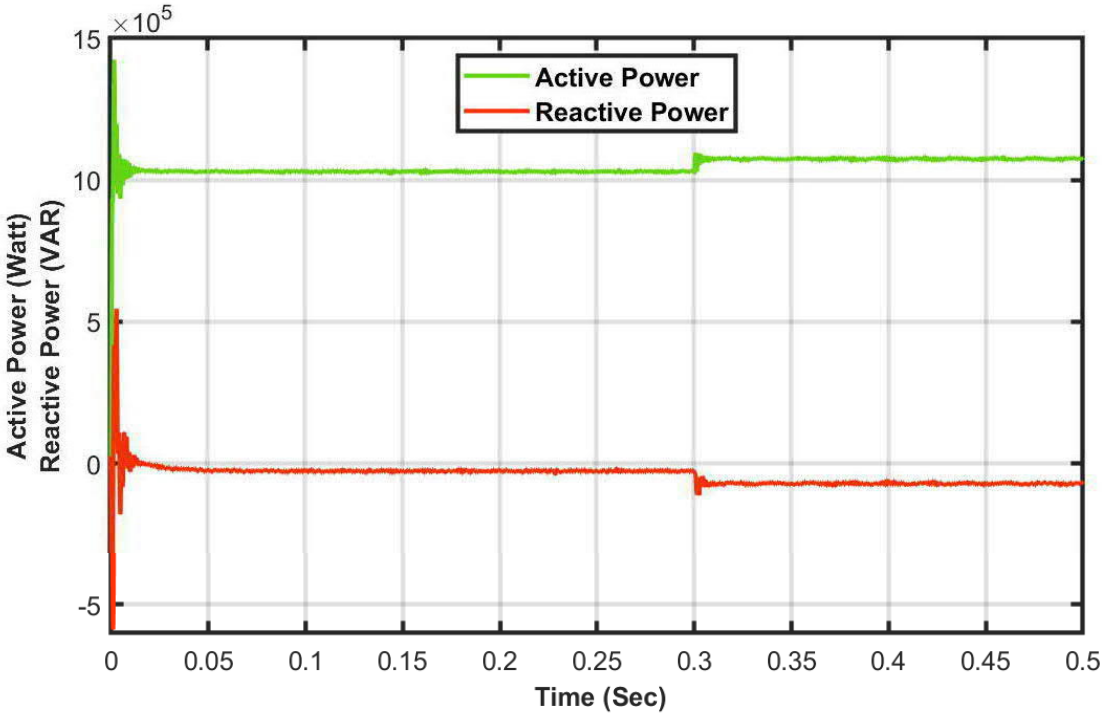

Figure 5.7 *Power condition when step change of increased grid voltage applied.*

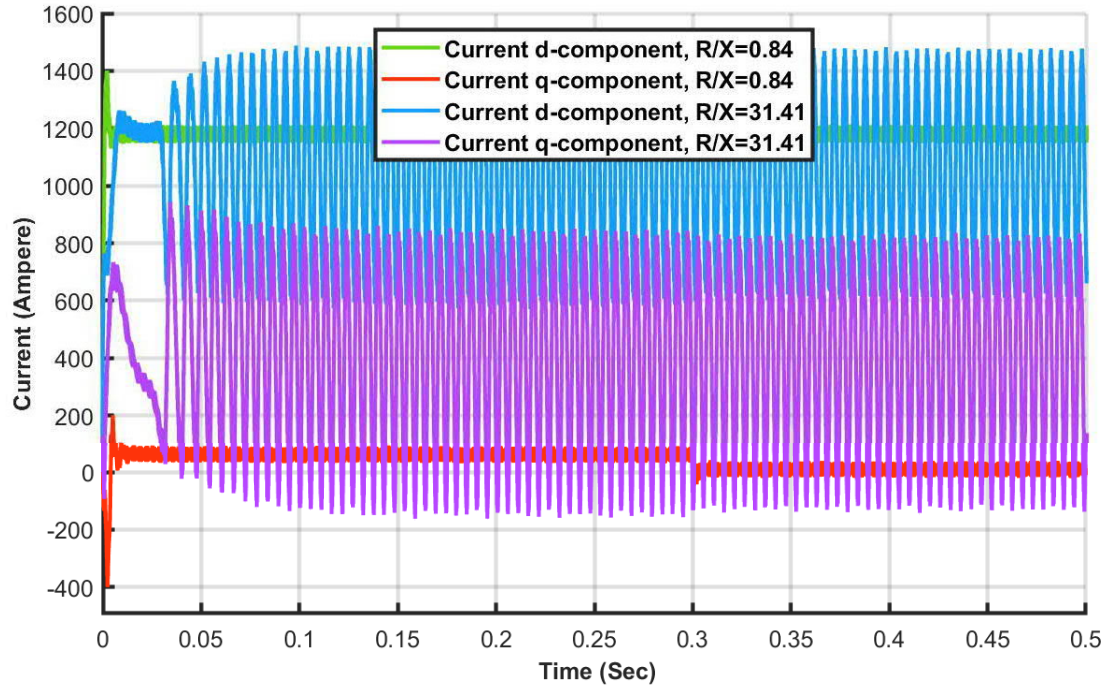

Figure 5.8 *Current condition at different* $\frac{R}{X}$ *when step change in grid voltage applied.*

of decreased grid voltage. In addition, Table 5.1, also illustrates the state of droop control for several $\frac{R}{X}$ ratio's.

Table 5.1 *Control state at different line resistances in medium voltage*

Resistance (R)	Reactance (X)	$\frac{R}{X}$	State
0.161Ω	0.191Ω	0.84	Stable
2Ω	0.191Ω	10.47	Stable
4Ω	0.191Ω	20.94	Stable
6Ω	0.191Ω	31.41	Unstable

5.2.2 Case B: Decreased grid voltage

In this case medium voltage grid is subjected to a step change of 5% below from the nominal value and the condition of q component current and corresponding reactive power is observed. Step change is applied at 0.3s of simulation time. The amount

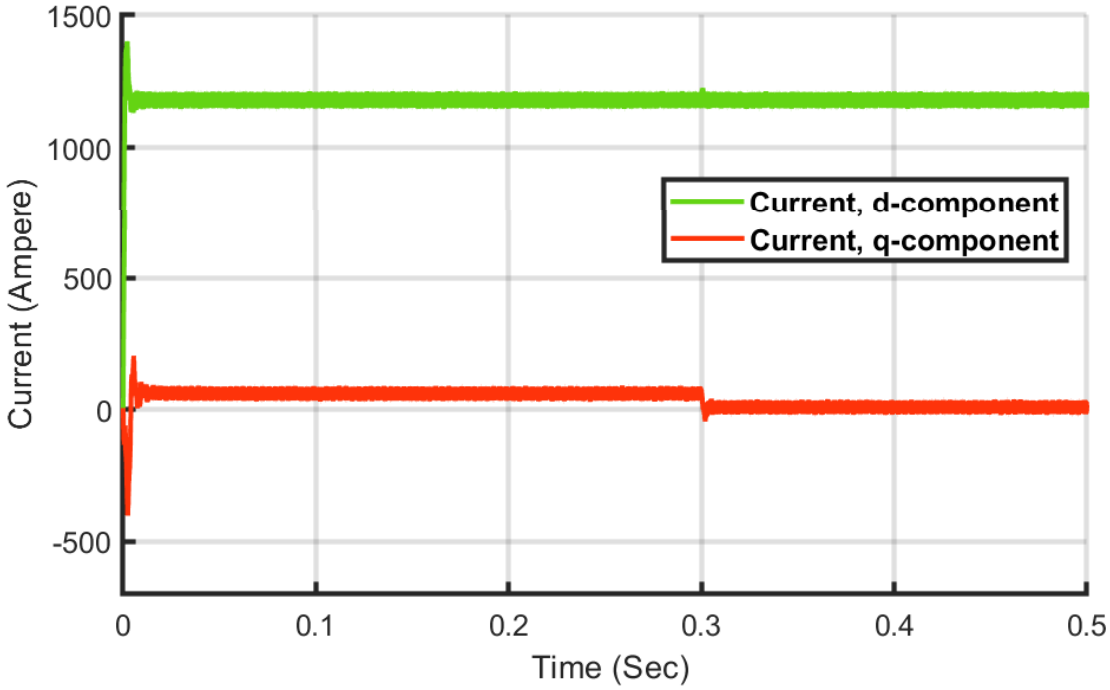

Figure 5.9 *Current condition when step change of decreased grid voltage applied.*

of q component current is negative after applying step change and it allows the converter to supply reactive power to the point of interconnection. This incident is observed from the Figure 5.9 and Figure 5.10.

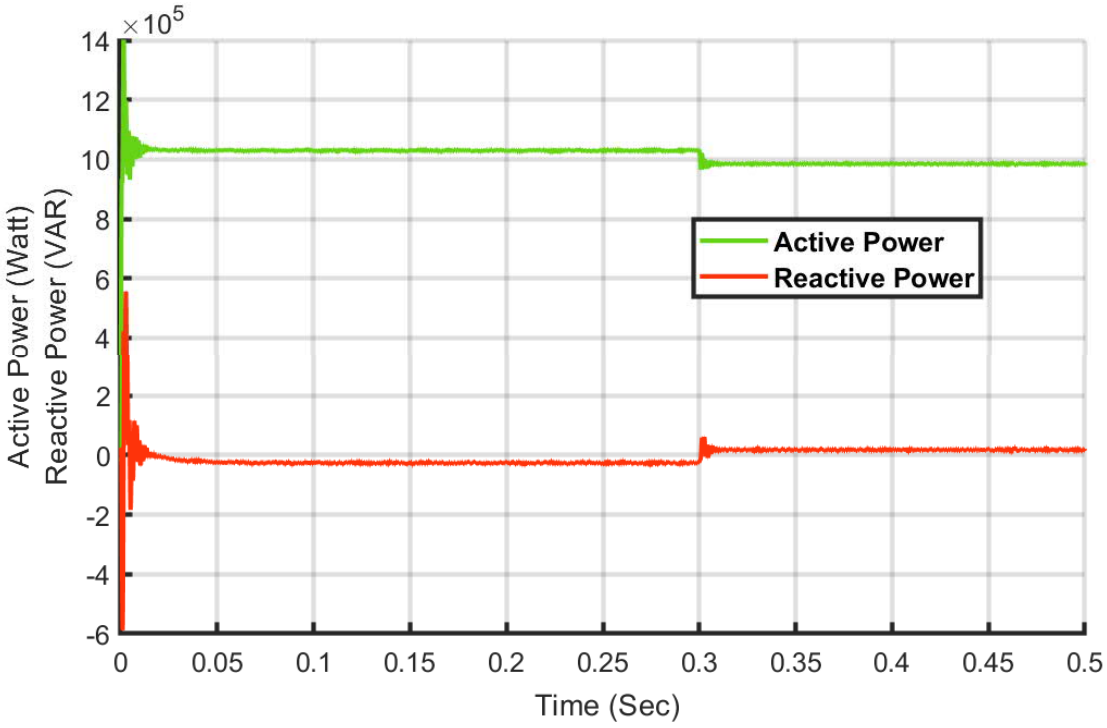

Figure 5.10 *Power condition when step change of decreased grid voltage applied*

5.3 Test case 3: Droop control verification in low voltage line.

To verify droop control in the low voltage transmission line, the converter model is connected to the 690 V AC grid through equivalent transmission line impedance. The transmission line has composed a resistance of 0.642 ohm/km and a reactance of 0.083 ohm/km and assuming that transmission line is 20 km long. Typically, short transmission line operated at the low voltage level. Observation of control performance is done by applying step change of 5% increased voltage in the grid. From Figure 5.11, it is noticed that d and q component of the converter current is oscillating. Converter d-component current is unable to keep track with its reference in the steady-state while q-component finds its reference generated from the droop controller with slight oscillation after 0.15 s of simulation time. Active and reactive power is coupled given in Figure 5.12, which indicates that droop is not working in this situation due to the high R/X ratio in the low voltage transmission line.

In this case, different line resistance and reactance are used later to find out the point where droop is stable in the low voltage transmission line. It is observed

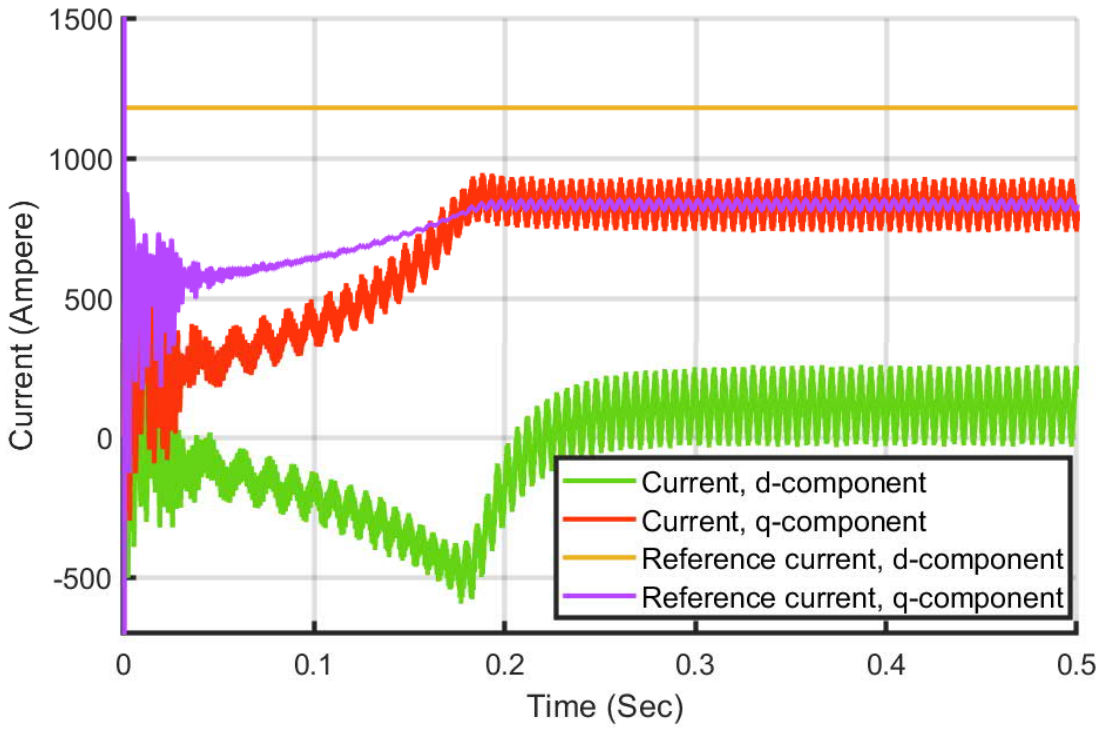

Figure 5.11 *Current condition when step change of increased grid voltage applied.*

that the converter is unstable with ideal line reactance which is used in low voltage transmission line even if without line resistance. In addition to that, the distance of the transmission line also effects on resistance and reactance appeared across the converter. Thus, stable operation of the converter at a specific R/X ratio does not mean that it would be stable at the same R/X ratio when transmission line distance increases or decreases. Table 5.2 and 5.3 given below, shows the control performance of the droop method while changing line impedance and distance.

Table 5.2 *Control state in low voltage at different $\frac{R}{X}$ in 20 km transmission line*

Resistance (R)	**Reactance (X)**	$\frac{\mathbf{R}}{\mathbf{X}}$	**Distance**	**State**
0.1Ω	0.0083Ω	12.04	20 km	Unstable
0.01Ω	0.0083Ω	1.2	20 km	Stable
0.641Ω	0.083Ω	7.7	20 km	Unstable

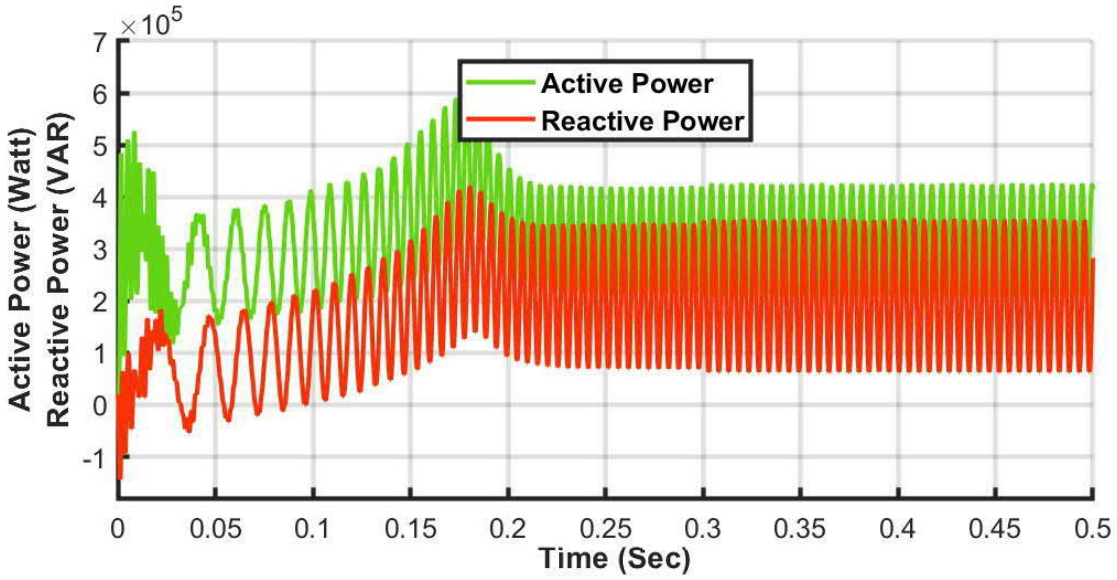

Figure 5.12 *Power condition when step change in grid voltage applied*

Table 5.3 *Control state in low voltage at different $\frac{R}{X}$ in 10 km transmission line*

Resistance (R)	**Reactance (X)**	$\frac{\mathbf{R}}{\mathbf{X}}$	**Distance**	**State**
0.1Ω	0.0083Ω	12.04	10 km	Stable
0.01Ω	0.0083Ω	1.2	10 km	Stable
0.641Ω	0.083Ω	7.7	10 km	Unstable

Power sharing condition is varied with the grid impedance. Active and reactive power sharing is not done by the contribution of fundamental voltage and current alone when grid impedance is resistive. Resistive gird impedance is summed up with the impedance of the LCL filter of the converter itself. This total impedance introduces harmonic resonance phenomena. Among the different order of harmonics, fourth order inter harmonic has a higher influence in converter output voltages and currents. Total harmonics distortion due to the harmonics presents in the converter output voltage and currents is exceeded IEEE standard. FFT analysis of the converter output voltages and currents are given in Figure 5.13 and 5.14 respectively.

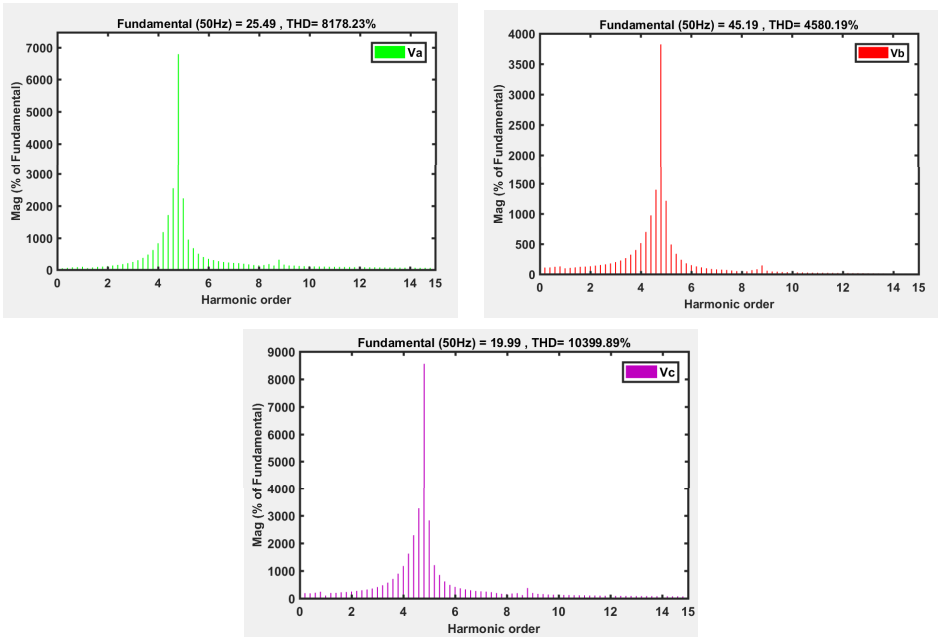

Figure 5.13 *Order of harmonics present in converter voltages*

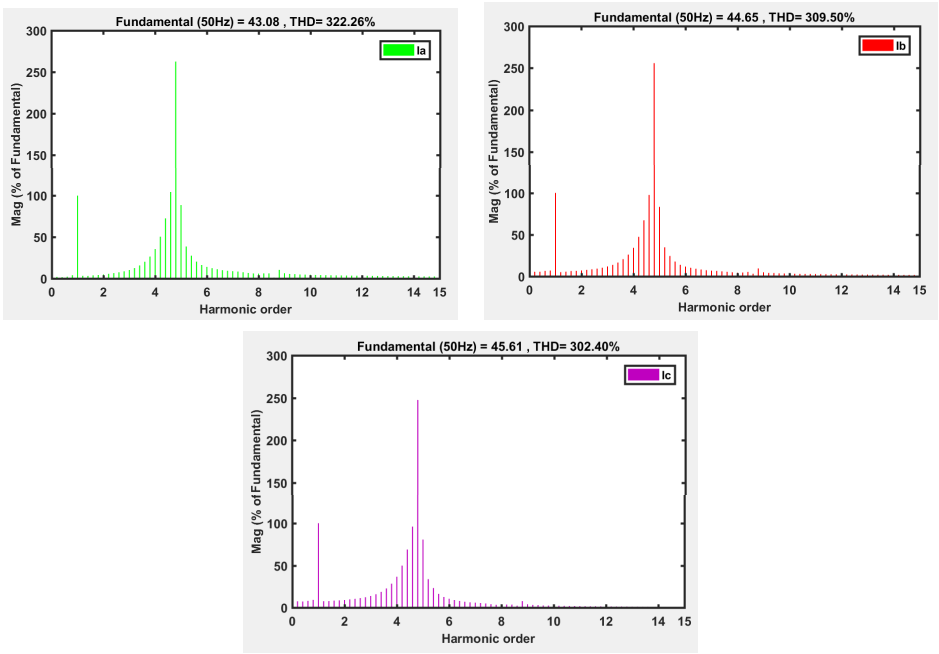

Figure 5.14 *Order of harmonics present in converter voltages*

5.4 Test case 4: Droop control verification in the IEEE-9 bus system.

The final test is done in an IEEE-9 bus topology. IEEE standard bus topology is used to test ideas and concepts by researchers. It is the high voltage network which is composed of 6, 230 KV high voltage bus and 3- generator bus. The necessary specification of the IEEE-9 bus system is given in the appendix. Additionally, a variable load of 10 MW active and 30 MVAr (inductive) load is connected to the bus-46. A switching mechanism is applied to connect the inductive load to observe the consequence of connecting the load at one of the high voltage buses. Bus number 4 is used in this regard. Later, another switching mechanism applied to connect the developed converter model to bus-4.

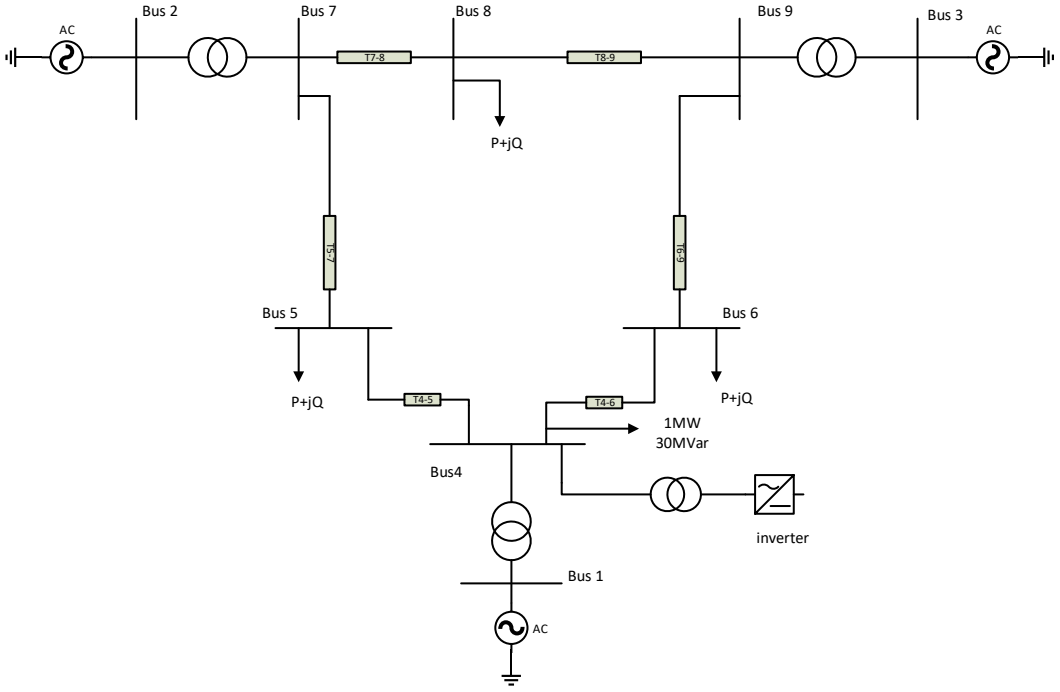

Figure 5.15 *IEEE-9 bus system used in test*

The designed model has the capacity of 50 KVAr which is very small to participate in a significant amount of reactive power compensation in the IEEE-9 bus network. To increase the reactive power sharing at the PCC, it is necessary to operate the converter at the lower power factor. At this stage, it is assumed that the converter is

operated at 0.85 power factor and the corresponding d and q component of current is calculated. Reactive power-sharing is done by controlling the q component within the calculated value, according to the droop method. Also, Ten number of low power factor converters are connected parallel first and then connected to bus-46 through a 690/230 KV step-up transformer. It is done to realize the effect of injecting reactive power on bus voltage as well. In bus-4, the load is connected after 0.2 s of simulation time and grid voltage without the inductive load is recorded. The recorded amplitude of the grid voltage is 156 KV. Later, grid voltage with the inductive load is observed until 0.4 s of simulation time. The observed grid voltage from 0.2 s-0.4 s simulation time is 147 KV. Finally, the designed converter is connected to the bus-4 at 0.4 s of simulation time and it is providing a sufficient amount of reactive power to improve the voltage profile of the bus-4 during the simulation time from 0.4 s-0.6 s. The grid voltage amplitude of 149 KV is recorded, which indicates that total of 2 KV improvement of grid voltage profile with the help of the converter connection is obtained. Figure 5.16 shows the grid voltage at bus-4 during the full simulation time.

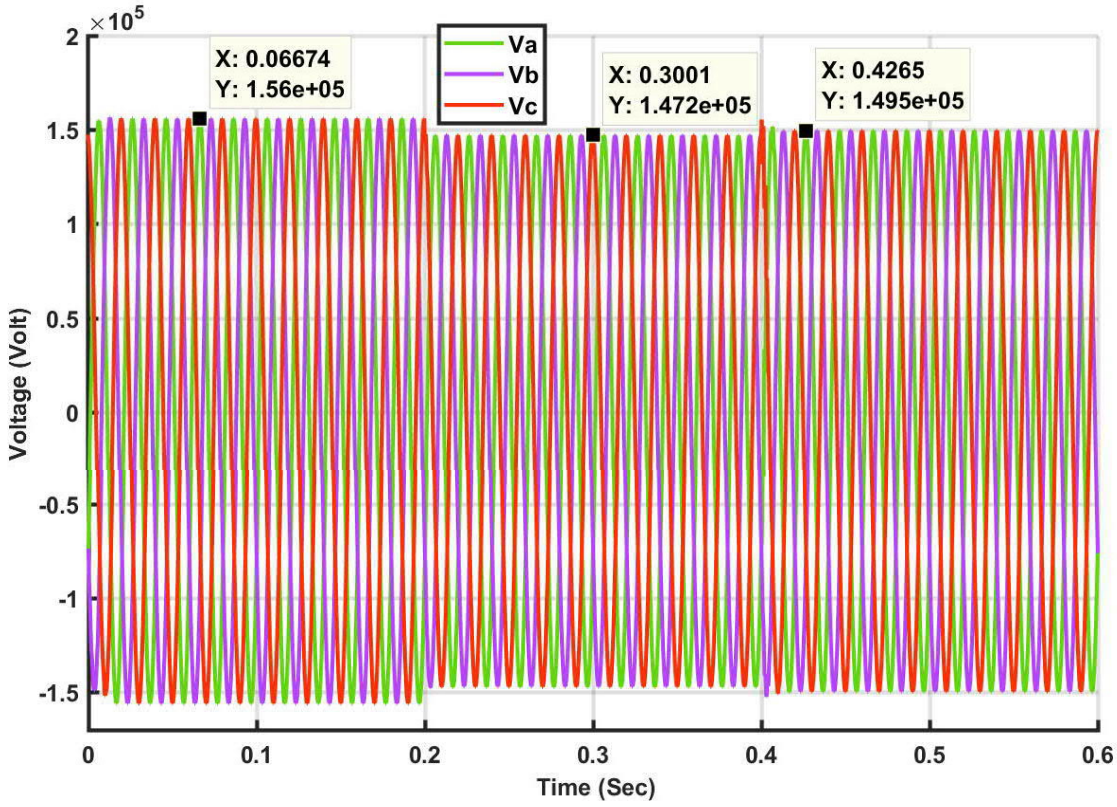

Figure 5.16 *Voltage profile of bus-46*

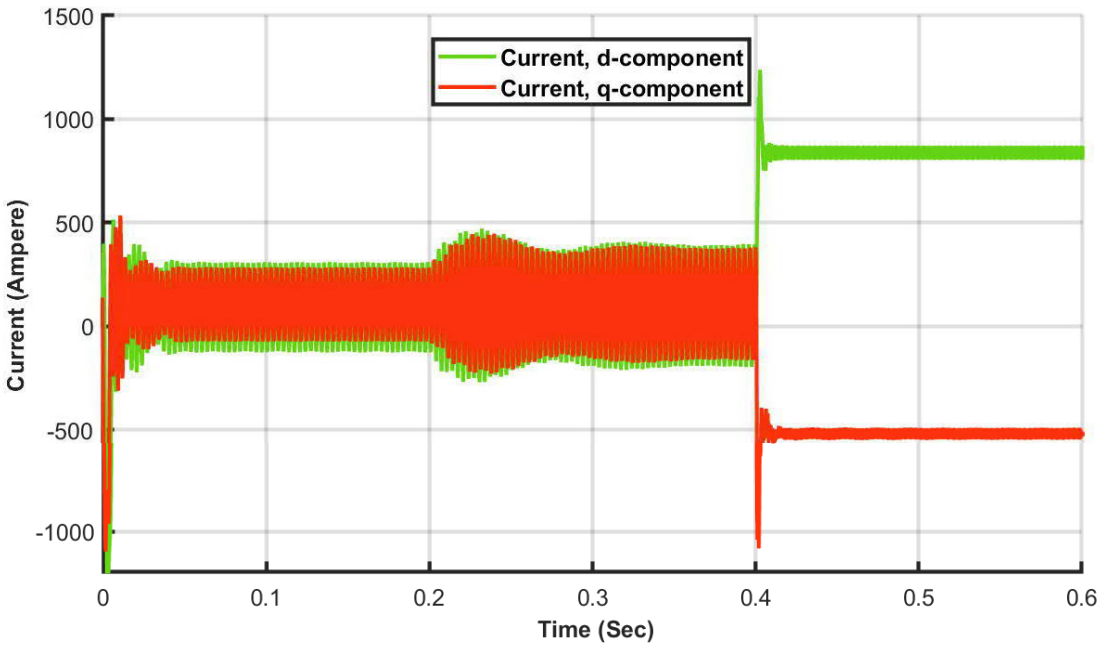

Figure 5.17 *Current condition when converter is connected with bus-4.*

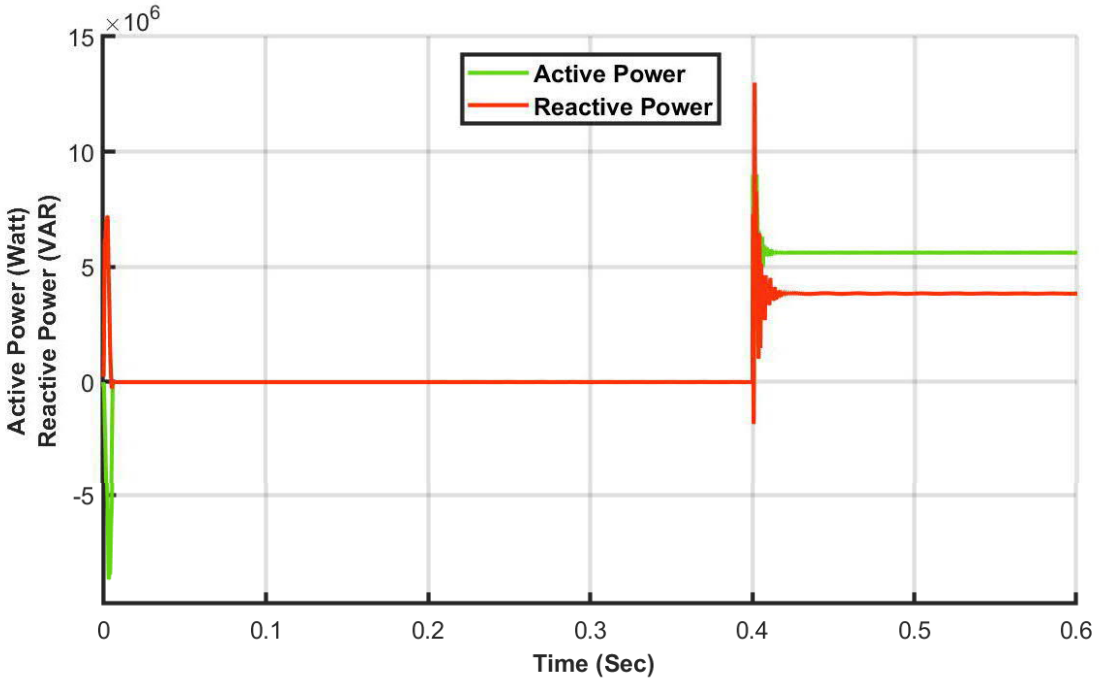

Figure 5.18 *Power condition when converter is connected with bus-4.*

Figure 5.17, it is observed that q component of the inner current controller is stable and the amount of the q component current is almost 540 A. This figure shows dq

component of the current of each 10 connected parallel converters during the simulation time. Ten identical converters are participating reactive power compensation and it is noticed form the power curve in Figure 5.18, which is positive 3.5 MVar. The positive sign of reactive power clearly indicates that 3.5 MVAr reactive power is supplied to the grid. This reactive power supply to the bus 4, help in minimizing voltage deviation due to the additional inductive load in bus 4.

5.5 Discussion

The achieved results from the different simulation can be analyzed through the mathematical behavior of droop control concerning low voltage, medium voltage, and high voltage transmission line. As the level of voltage decreases, the more resistivity comes into play in the transmission line. Thus, power-sharing through grid-connected converter is difficult in low voltage grid. Further mathematical illustration and interpretation are given below.

- Power flow through the line impedance : Real and reactive power feeding to the grid can be calculated using the simple single diagram presented in Figure 5.19. Applying Kirchhoff's voltage law in the in Figure 5.19, the amount of current flowing through the converter to the grid is obtained.

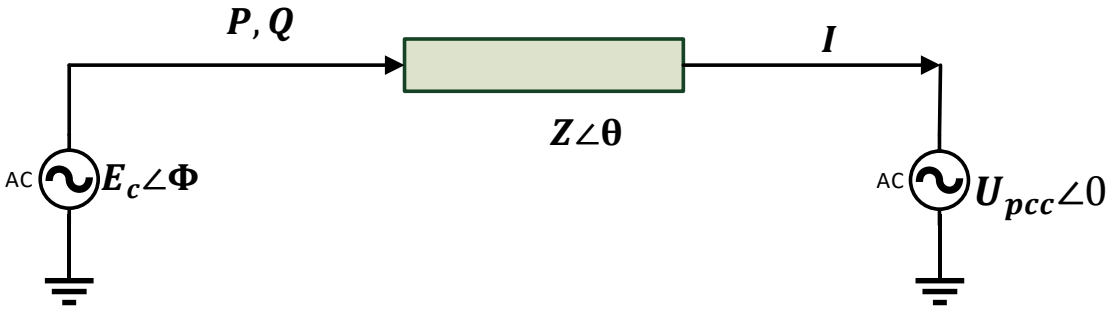

Figure 5.19 *Converter supplying power to the grid*

$$\mathbf{E}_c - \mathbf{ZI} - \mathbf{U}_{PCC} = 0 \tag{5.1}$$

$$\begin{aligned}\mathbf{I} &= \frac{\mathbf{E}_c - \mathbf{U}_{PCC}}{\mathbf{Z}} \\ \mathbf{I} &= \frac{E_c\angle\phi - U_{PCC}\angle 0}{Z\angle\theta} \\ \mathbf{I} &= \frac{E_c}{Z}\angle\phi - \theta - \frac{U_{PCC}}{Z}\angle -\theta\end{aligned} \tag{5.2}$$

Complex power of the single line can be obtained in (5.3) by replacing current conjugate found in (5.2)

$$\begin{aligned}\mathbf{S} &= \mathbf{E}_c\mathbf{I}^* \\ &= E_c\angle\phi\big(\frac{E_c}{Z}\angle(\theta-\phi) - \frac{U_{PCC}}{Z}\angle\theta\big) \\ &= \frac{E_c^2}{Z}\angle\theta - \frac{U_{PCC}E_c}{Z}\angle\theta + \phi \\ &= \frac{E_c^2}{Z}\cos\theta + j\frac{E_c^2}{Z}\sin\theta - \frac{U_{PCC}E_c}{Z}\cos(\theta+\phi) - j\frac{U_{PCC}E_c}{Z}\sin(\theta+\phi)\end{aligned} \tag{5.3}$$

Expressing real and reactive power separately in equation (5.4) and (5.5)

$$\begin{aligned}P &= \frac{E_c^2}{Z}\cos\theta - \frac{U_{PCC}E_c}{Z}\cos(\theta+\phi) \\ &= \frac{E_c^2}{Z}\cos\theta - \frac{U_{PCC}E_c}{Z}\big(\cos\theta\cos\phi - \sin\theta\sin\phi\big) \\ &= \cos\theta\left(\frac{E_c^2}{Z} - \frac{U_{PCC}E_c}{Z}\cos(\phi)\right) + \frac{U_{PCC}E_c}{Z}\sin\theta\sin\phi\end{aligned} \tag{5.4}$$

$$\begin{aligned}Q &= \frac{E_c^2}{Z}\sin\theta - \frac{U_{PCC}E_c}{Z}\sin(\theta+\phi) \\ &= \frac{E_c^2}{Z}\sin\theta - \frac{U_{PCC}E_c}{Z}\big(\sin\theta\cos\phi + \cos\theta\sin\phi\big) \\ &= \sin\theta\left(\frac{E_c^2}{Z} - \frac{U_{PCC}E_c}{Z}\cos(\phi)\right) - \frac{U_{PCC}E_c}{Z}\cos\theta\sin\phi\end{aligned} \tag{5.5}$$

If the phase angle ϕ is too small then, $\sin\phi$ and $\cos\phi$ can be replaced by ϕ and 1 respectively in equation (5.4) and (5.5). Simplified equation is given in equation (5.6) and (5.7)

$$P = \cos(\theta)\left(\frac{E_c^2}{Z} - \frac{U_{PCC}E_c}{Z}\right) + \frac{U_{PCC}E_c}{Z}\sin(\theta)\phi \tag{5.6}$$

$$Q = \sin(\theta)\left(\frac{E_c^2}{Z} - \frac{U_{PCC}E_c}{Z}\right) - \frac{U_{PCC}E_c}{Z}\cos(\theta)\phi \tag{5.7}$$

- Power flow when the line impedance is inductive : When the transmission line is highly inductive then, it is relevant that θ approaches to $\frac{\pi}{2}$. The real power and reactive power in equation (5.6) and (5.7) is again simplified as equation (5.8) and (5.9).

$$P = \frac{U_{PCC}E_c}{X}\phi \tag{5.8}$$

$$\begin{aligned} Q &= \frac{E_c^2}{X} - \frac{U_{PCC}E_c}{X} \\ &= \frac{E_c(E_c - U_{PCC})}{X} \end{aligned} \tag{5.9}$$

  Equation (5.9) if, $U_{PCC} \gg E_C$ then, the amount of reactive power is negative, this implies that reactive power should be absorbed by the converter in order to limit the voltage limit at the PCC and vice versa. On the other hand, real power depends on the phase angle of the converter. In other words, real power can be controlled by controlling frequency.

- Power flow when the line impedance is Resistive : When the transmission line is highly resistive then, it is relevant that θ approaches to 0. The real power and reactive power in equation (5.6) and (5.7) is again simplified as equation (5.10) and (5.11).

$$\begin{aligned} P &= \frac{E_c^2}{X} - \frac{U_{PCC}E_c}{R} \\ &= \frac{E_c(E_c - U_{PCC})}{X} \end{aligned} \tag{5.10}$$

$$Q = \frac{U_{PCC}E_c}{R}\phi \tag{5.11}$$

  Now, equation (5.10) and (5.11) shows the reverse phenomena from the previous case. The amount of reactive power injection depends on frequency and real power depends on the voltage drop over the line impedance.

The conventional droop characteristics work only when the line impedance is inductive. Thus, the droop control mechanism applied to the controlling of reactive power is possible when the grid-connected converter is connected to the medium voltage and high voltage grid through the transmission line. The droop control does not necessarily work on reactive power control for the low voltage grid.

6. CONCLUSION

The tendency of using grid-connected converter especially voltage source converter as a power quality improvement device is observed through literature studies. Reactive power control ability of grid converter usually supports the grid, particularly to avoid voltage sag and swell at the point of common coupling. It is not so difficult in the synchronous reference frame and using a simple PI controller. This is because active and reactive power can be controlled independently by controlling d and q component of converter generated current. An outer controller is required for generating reactive current according to the grid condition. This generated current is used as a reference current for the inner current PI controller. Thus, inner control function acts in a way that converter either supplies or absorbs the same amount of current that is generated by the outer controller. Controller parameter is defined using the Q-V droop mechanism due to its simple and easy implementation.

A simulation model of MW level inverter is designed to control reactive power using Q-V droop mechanism. The defined architecture of the inverter is two level three-phase inverter intending to test low medium and high voltage grid. Thus, in high voltage application, it is necessary to use a transformer for stepping up the voltage from a designed architecture which is compatible with the low voltage grid in transformer-less connection. In order to supply quality power to the grid, LCL filtering technique is used to reduce harmonics produced by converter switching. However, LCL filtering technique may introduce resonance peaking. It may be reduced by using a damping resistor. In order to analyze the control mechanism and to ensure the controller stability small signal modeling of the converter is done. Small signal modeling of the converter is complex with the aim of controlling reactive power. It is getting more complex when there is an LCL filtering is involved in the filtering. Few assumptions have been made for making the calculation easy. Finally, The transfer functions G_{cld-0} and G_{clq-0} is obtained for the inner current control of d and q component of the converter current.

To implement the reactive power control in a simulation environment, the block diagram is developed where, all control blocks are illustrated. An SRF-PLL is used to synchronize the converter with the grid. In SRF-PLL a PI controller is used to works on error signal produced from the comparison of q component of grid voltage and the reference value. The reference is usually set to zero. controller with low cross-over frequency is used here to avoid impedance based interaction and to operate the PI controller used in the stable state.

In inner current control, two PI controller is used to control generated current from the converter which is flowing through the converter side inductor. PI controller works on an error signal which is generated from the comparison of q or d component of the converter current and their steady-state values. If the converter operates at zero power factor then reference of q channel PI controller is set to zero, otherwise, it has to be set according to the reactive power generation requirement. The usage of higher control bandwidth for faster control dynamics is limited due to the resonance peaking caused by LCL filter. The control bandwidth less than the resonant frequency is used in order to avoid instability due to LCL filtering. The controller tuning is done by using the loop shaping technique.

In order to regulate reactive power, an outer controller is designed to generate the q-channel current reference. The outer controller is designed according to the Q-V droop characteristics which are analogous to synchronous generator voltage control. In Q-V droop, the reactive power requirement is set by the voltage deviation from the preferred level. If the voltage deviation is negative, the certain amount of reactive power should be drawn and vice versa. Since Q-V droop shows proportionality behavior, a proportional controller should be designed. The process of selecting the gain of that controller is discussed in Chapter 4.

The designed model with all control functionalities is then tested in few several test cases. Test case shows that droop control works fine when the converter supplies power through high and medium voltage transmission line. However, it does not work with the low voltage transmission line. It is studied that, resistivity increases with the decrease of the level of voltage. When a transmission line with a high resistivity connect to the converter the reactive and active power dependency flowing through the transmission line is altered. The regulation of reactive power previously depends on voltage now depends on the frequency with the transmission line of high resistivity. A practical simulation experiment with IEEE-9, high voltage bus system

is done later. The results show that the performance of droop control is well in that case. However, the lower rating of the designed converter is not enough to see the visible reactive power control action. Thus, several identically designed converter then connected in parallel to the grid bus. This step affects the reactive power regulating accuracy. The power loss due to the circulating current among the parallel connected converters might be one of the reason.

BIBLIOGRAPHY

[1] A. S. Anees, "Grid integration of renewable energy sources: Challenges, issues and possible solutions," in *Power Electronics (IICPE), 2012 IEEE 5th India International Conference on*. IEEE, 2012, pp. 1–6.

[2] H. Awad and M. H. Bollen, "Power electronics for power quality improvements," in *Industrial Electronics, 2003. ISIE'03. 2003 IEEE International Symposium on*, vol. 2. IEEE, 2003, pp. 1129–1136.

[3] A. Milczarek, M. Malinowski, and J. M. Guerrero, "Reactive power management in islanded microgrid—proportional power sharing in hierarchical droop control," *IEEE Transactions on Smart Grid*, vol. 6, no. 4, pp. 1631–1638, 2015.

[4] M. Stanojević, K. Kasaš-Lažetić, N. Đurić, and M. Prša, "Analysis of generalized droop control in medium and low voltage power electric grids," in *Industrial Electronics (INDEL), International Symposium on*. IEEE, 2016, pp. 1–6.

[5] F. Blaabjerg, Z. Chen, and S. B. Kjaer, "Power electronics as efficient interface in dispersed power generation systems," *IEEE transactions on power electronics*, vol. 19, no. 5, pp. 1184–1194, 2004.

[6] X. Wang, Y. W. Li, F. Blaabjerg, and P. C. Loh, "Virtual-impedance-based control for voltage-source and current-source converters," *IEEE Trans. Power Electron*, vol. 30, no. 12, pp. 7019–7037, 2015.

[7] S. Azmi, K. Ahmed, S. Finney, and B. Williams, "Comparative analysis between voltage and current source inverters in grid-connected application," 2011.

[8] E. Acha, C. R. Fuerte-Esquivel, H. Ambriz-Perez, and C. Angeles-Camacho, *FACTS: modelling and simulation in power networks*. John Wiley & Sons, 2004.

[9] S. Kirmani and B. Kumar, "Power quality improvement by using statcom control scheme in wind energy generation interface to grid," *Journal of Contemporary Urban Affairs*, vol. 1, no. 3, pp. 31–37, 2017.

[10] M. Iorgulescu and D. Ursu, "Reactive power control and voltage stability in power systems," in *Reactive Power Control in AC Power Systems*. Springer, 2017, pp. 227–248.

[11] N. Flourentzou, V. G. Agelidis, and G. D. Demetriades, "Vsc-based hvdc power transmission systems: An overview," *IEEE Transactions on power electronics*, vol. 24, no. 3, pp. 592–602, 2009.

[12] S. Ruihua, Z. Chao, L. Ruomei, and Z. Xiaoxin, "Vscs based hvdc and its control strategy," in *Transmission and Distribution Conference and Exhibition: Asia and Pacific, 2005 IEEE/PES*. IEEE, 2005, pp. 1–6.

[13] J. Rocabert, A. Luna, F. Blaabjerg, and P. Rodriguez, "Control of power converters in ac microgrids," *IEEE transactions on power electronics*, vol. 27, no. 11, pp. 4734–4749, 2012.

[14] A. Egea-Alvarez, A. Junyent-Ferré, and O. Gomis-Bellmunt, "Active and reactive power control of grid connected distributed generation systems," in *Modeling and control of sustainable power systems*. Springer, 2012, pp. 47–81.

[15] J. L. Dominguez-Garcia, F. Bianchi, and O. Gomis, "Power control of voltage source converter for distributed generation," 2011.

[16] P. Agarwal and R. Gupta, "Grid integration of solar pv power using shunt connected vsc," in *Engineering and Systems (SCES), 2013 Students Conference on*. IEEE, 2013, pp. 1–6.

[17] X. Meng, Z. Liu, J. Liu, T. Wu, S. Wang, and B. Liu, "Comparison between virtual synchronous generator and droop controlled inverter," in *Power Electronics Conference (SPEC), IEEE Annual Southern*. IEEE, 2016, pp. 1–6.

[18] Q.-C. Zhong and G. Weiss, "Synchronverters: Inverters that mimic synchronous generators," *IEEE Transactions on Industrial Electronics*, vol. 58, no. 4, pp. 1259–1267, 2011.

[19] B. Zhang, X. Yan, D. Li, X. Zhang, J. Han, and X. Xiao, "Stable operation and small-signal analysis of multiple parallel dg inverters based on a virtual synchronous generator scheme," *Energies*, vol. 11, no. 1, p. 203, 2018.

[20] H. Liu, L. Yu, H. Wu, G. Liu, and W. Wang, "Small signal modeling and stability analysis on parallel photovoltaic inverters in microgrid," in *Energy Conversion Congress and Exposition (ECCE), 2015 IEEE*. IEEE, 2015, pp. 3754–3759.

[21] U. B. Tayab, M. A. B. Roslan, L. J. Hwai, and M. Kashif, "A review of droop control techniques for microgrid," *Renewable and Sustainable Energy Reviews*, vol. 76, pp. 717–727, 2017.

[22] E. Planas, A. Gil-de Muro, J. Andreu, I. Kortabarria, and I. M. de Alegría, "General aspects, hierarchical controls and droop methods in microgrids: A review," *Renewable and Sustainable Energy Reviews*, vol. 17, pp. 147–159, 2013.

[23] P. Kundur, N. J. Balu, and M. G. Lauby, *Power system stability and control*. McGraw-hill New York, 1994, vol. 7.

[24] T. Suntio, T. Messo, and J. Puukko, *Power Electronic Converters: Dynamics and Control in Conventional and Renewable Energy Applications*. John Wiley & Sons, 2017.

[25] I. Cvetkovic, M. Jaksic, D. Boroyevich, P. Mattavelli, F. C. Lee, Z. Shen, S. Ahmed, and D. Dong, "Un-terminated, low-frequency terminal-behavioral dq model of three-phase converters," in *Energy Conversion Congress and Exposition (ECCE), 2011 IEEE*. IEEE, 2011, pp. 791–798.

[26] H. M. Ahn, C.-Y. Oh, W.-Y. Sung, J.-H. Ahn, and B. K. Lee, "Analysis and design of lcl filter with passive damping circuits for three-phase grid-connected inverters," *Journal of Electrical Engineering & Technology*, vol. 12, no. 1, pp. 217–224, 2017.

[27] X. Ruan, X. Wang, D. Pan, D. Yang, W. Li, and C. Bao, "Design of lcl filter," in *Control Techniques for LCL-Type Grid-Connected Inverters*. Springer, 2018, pp. 31–61.

[28] K. Jalili and S. Bernet, "Design of *lcl* filters of active-front-end two-level voltage-source converters," *IEEE Transactions on Industrial Electronics*, vol. 56, no. 5, pp. 1674–1689, 2009.

[29] H. Yuan and X. Jiang, "A simple active damping method for active power filters," in *Applied Power Electronics Conference and Exposition (APEC), 2016 IEEE*. IEEE, 2016, pp. 907–912.

[30] M. Liserre, F. Blaabjerg, and S. Hansen, "Design and control of an lcl-filter-based three-phase active rectifier," *IEEE Transactions on industry applications*, vol. 41, no. 5, pp. 1281–1291, 2005.

[31] M. A. Mosa, A. A. Elsyed, A. M. Amin, and A. A. Ghany, "Modified design of an lcl filter for grid-connected, pulse-width-modulated voltage source converter," in *Power Systems Conference (MEPCON), 2016 Eighteenth International Middle East*. IEEE, 2016, pp. 89–94.

[32] A. Reznik, M. G. Simões, A. Al-Durra, and S. Muyeen, "*lcl* filter design and performance analysis for grid-interconnected systems," *IEEE Transactions on Industry Applications*, vol. 50, no. 2, pp. 1225–1232, 2014.

[33] S. Seo, Y. Cho, and K.-B. Lee, "Lcl-filter design for grid-connected three-phase inverter using space vector pwm," in *Power Electronics and Motion Control Conference (IPEMC-ECCE Asia), 2016 IEEE 8th International*. IEEE, 2016, pp. 389–394.

[34] T. C. Wang, Z. Ye, G. Sinha, and X. Yuan, "Output filter design for a grid-interconnected three-phase inverter," in *Power Electronics Specialist Conference, 2003. PESC'03. 2003 IEEE 34th Annual*, vol. 2. IEEE, 2003, pp. 779–784.

[35] D. N. Zmood and D. G. Holmes, "Stationary frame current regulation of pwm inverters with zero steady-state error," *IEEE Transactions on power electronics*, vol. 18, no. 3, pp. 814–822, 2003.

[36] S. Bhattacharya and D. Divan, "Synchronous frame based controller implementation for a hybrid series active filter system," in *Industry Applications Conference, 1995. Thirtieth IAS Annual Meeting, IAS'95., Conference Record of the 1995 IEEE*, vol. 3. IEEE, 1995, pp. 2531–2540.

[37] P. P. Dash and M. Kazerani, "Dynamic modeling and performance analysis of a grid-connected current-source inverter-based photovoltaic system," *IEEE Transactions on Sustainable Energy*, vol. 2, no. 4, pp. 443–450, 2011.

[38] M. Judewicz, S. González, J. Fischer, J. Martínez, and D. Carrica, "Inverter-side current control of grid-connected voltage source inverters with lcl filter based on generalized predictive control," *IEEE Journal of Emerging and Selected Topics in Power Electronics*, 2018.

[39] L. Bede, G. Gohil, T. Kerekes, M. Ciobotaru, R. Teodorescu, and V. G. Agelidis, "Comparison between grid side and inverter side current control for parallel interleaved grid connected converters," in *Power Electronics and Applications*

(EPE'15 ECCE-Europe), 2015 17th European Conference on. IEEE, 2015, pp. 1–10.

[40] A. Aapro, "Modeling dynamics of photovoltaic inverter with lcl-type grid filter," 2014.

[41] N. Jaalam, N. Rahim, A. Bakar, C. Tan, and A. M. Haidar, "A comprehensive review of synchronization methods for grid-connected converters of renewable energy source," *Renewable and Sustainable Energy Reviews*, vol. 59, pp. 1471–1481, 2016.

[42] S. K. Subramanium, *Investigation on grid synchronization methods in grid connected pv inverters during unbalanced condition*, Tampere University of Technology, 2015.

[43] T. Messo, J. Jokipii, A. Makinen, and T. Suntio, "Modeling the grid synchronization induced negative-resistor-like behavior in the output impedance of a three-phase photovoltaic inverter," in *Power Electronics for Distributed Generation Systems (PEDG), 2013 4th IEEE International Symposium on*. IEEE, 2013, pp. 1–7.

[44] T. Suntio, *Dynamic profile of switched-mode converter: modeling, analysis and control*. John Wiley & Sons, 2009.

[45] M. A. Hossain, H. R. Pota, W. Issa, and M. J. Hossain, "Overview of ac microgrid controls with inverter-interfaced generations," *Energies*, vol. 10, no. 9, p. 1300, 2017.

[46] J. Pegueroles Queralt, F. D. Bianchi, and O. Gomis Bellmunt, "Optimal droop control for voltage source converters in islanded microgrids," in *8th PIFAC Proceedings Volumes (IFAC-PapersOnline) Control Symposium, PPPSC 2012*, 2012, pp. 566–571.

APPENDIX A. INFORMATION ON IEEE-9 BUS

Table 1 *IEEE-9 bus specification*

Bus number	**Bus Voltage (KV)**	**Phase angle (deg)**
1	16	00
2	18	9.17
3	13.8	4.56
4	230	−2.23
5	230	−4
6	230	−3.70
7	230	3.62
8	230	0.63
9	230	1.87

Although bus number 4 has the voltage level of 230 KV, when simulation starts without load and converter, it shows the voltage level of 156 KV.